JOURNAL OF PETROLOGY | VOLUME 47 | NUMBER 9 | PAGES 1809–1851 | 2006 | doi:10.1093/petrology/egl028

Mechanism of Crystal Redistribution in a Sheet-like Magma Body: Constraints from the Nosappumisaki and Other Shoshonite Intrusions in the Nemuro Peninsula, Northern Japan

RAYKO SIMURA* AND KAZUHITO OZAWA

DEPARTMENT OF EARTH AND PLANETARY SCIENCE, GRADUATE SCHOOL OF SCIENCE, THE UNIVERSITY OF TOKYO, HONGO 7-3-1, BUNKYO-KU, TOKYO 113-0033, JAPAN

RECEIVED APRIL 15, 2005; ACCEPTED APRIL 10, 2006; ADVANCE ACCESS PUBLICATION MAY 11, 2006

Processes of crystal separation in a magma heavily laden with crystals without phase change are investigated from observations on frozen magma systems: Nosappumisaki and other shoshonite intrusions in the Nemuro peninsula, Japan, for which the origin of the crystals and the initial conditions are well constrained. The Nosappumisaki intrusion is 120 m in thickness and extends for more than 1·5 km. It exhibits a wide range of lithological variation, principally as a result of crystal redistribution after intrusion. Crystals in each lithology can be clearly divided into two kinds according to their composition and texture: those present before the intrusion of the magma ('phenocrysts') and those that crystallized in situ *after intrusion. From the vertical change in mode and size of 'phenocrysts', it is shown that (1) augite 'phenocrysts' were rapidly deposited, with little overgrowth after intrusion, by significant coagulation or clustering on a time-scale of more than a few years, and (2) plagioclase 'phenocrysts', definitely denser than the melt but concentrated in the upper level, floated by counter flow of massive deposition of augite 'phenocrysts'. These results indicate that in a magma heavily laden with crystals of a few millimeters in size (>20 vol. %), crystal–crystal and crystal–melt interaction play an important role in the separation of crystals from the host melt.*

KEY WORDS: *magma chamber; sill; crystal settling; plagioclase flotation; Nosappumisaki*

INTRODUCTION

Magmatic fractionation plays a central role in the chemical and structural evolution of the Earth's crust. It proceeds through intimate interaction between crystallization and separation of crystals from residual melt (e.g. Bowen, 1928; Marsh, 1996). To understand this interaction, it is essential to clarify the mechanism of melt–crystal separation as well as heat transportation and the thermodynamics and kinetics of the magmatic system (e.g. Kirkpatrick *et al.*, 1976; Ghiorso & Sack, 1995).

Mechanisms of particle transportation (settling or flotation) in liquids without phase changes have been examined in many experimental and theoretical studies in the engineering field. Crystal transportation in dilute suspension, in which the crystals are far apart from each other, can be treated as transportation of a single particle. If the particle is spherical, it follows the Stokes' settling law (Stokes, 1851) if the fluid behaves as a Newtonian fluid. The effects of crystal shape in dilute suspensions have been considered with the Stokes' settling formulation by many researchers (e.g. Jeyaweera & Mason, 1965; Kerr & Lister, 1991; Hartman *et al.*, 1994). In concentrated suspensions, the distance between the crystals becomes shorter and their interaction cannot be neglected. This interaction has been investigated from

*Corresponding author. Present address, Fukuda Laboratory, Institute of Multidisciplinary Research for Advanced Materials, Tohoku University, Katahira 2-1-1, Aoba-ku, Sendai 980-8577, Japan. Telephone: +81-22-217-5167. Fax: +81-22-215-5102. E-mail: ray@tagen.tohoku.ac.jp

various points of view, such as particle concentration (Richardson & Zaki, 1954; Barnea & Mizrahi, 1973), particle size distribution (Lockett & Al-Habbooby, 1973, 1974; Greenspan & Ungarish, 1982), and the mechanics of direct interaction between particles (Stimson & Jeffery, 1926; Saffman, 1973; Wacholder & Sather, 1974; Batchelor, 1982; Jeffrey & Onishi, 1984; Han & Lawler, 1991). Many other studies on particle transportation in liquids without phase changes have been carried out; for instance, on the effects of poly-particle suspensions with different density and size (Kynch, 1958; Richardson & Meikle, 1961; Masliyah, 1979; Davis & Gecol, 1994; Doheim *et al.*, 1997; Bürger *et al.*, 2000), the effects of cluster formation (Kaye & Boardman, 1962; Schwindinger, 1999) and the effects of thermal convection (Jaupart *et al.*, 1984; Jaupart & Brandeis, 1986; Martin & Nokes, 1988, 1989; Brandeis & Marsh, 1989; Kerr *et al.*, 1989; Koyaguchi *et al.*, 1993).

Crystal transportation in an actual magmatic system is, however, strongly affected by crystallization induced by heat transport, and it is fairly difficult to fully understand the whole process. One way to overcome this difficulty is to investigate crystal transportation that can be regarded as independent from crystallization. Such a situation is realized when the time-scale of crystal transportation is much shorter than that of the total solidification. An ideal situation would be if the transported crystals were sequentially frozen in the peripheral regions of a magma body with limited nucleation and overgrowth on the crystals initially present in the central part. Two studies following this strategy, on the basis of natural observations, are those of Gray & Crain (1969) and Fujii (1974). Fujii (1974) estimated the settling time-scale of olivine crystals based on the vertical variation of olivine modal abundance in a dolerite sill, in which the crystals were interpreted to have been already present at the time of intrusion because of their presence in the chilled margin. Fujii, however, assumed that the olivine crystals were homogeneously distributed in the magma in the beginning and that crystal settling was according to Stokes' Law without further growth and was frozen by conductive cooling. This simplified model could reproduce the vertical variation of olivine abundance, but is not consistent with the absence of size grading that would be inevitable if crystal settling obeyed Stokes' Law. This suggests the operation of other settling mechanisms such as direct (e.g. collision) or indirect (through melt flow) crystal–crystal interactions, which become effective if the crystal fraction is greater than 0·01 (Davis & Acrivos, 1985). These mechanisms affect the vertical variation of crystal size distribution as well as the time-scale of crystal settling. Even if we can ignore thermal convection and crystallization, quantitative evaluation of the direct or indirect interaction between crystals is necessary to understand the general transportation mechanism of crystals in a magmatic system.

The purpose of this study is to present observations from fossil magma storage systems, Cretaceous shoshonite intrusions in the Nemuro peninsula, northern Japan, which can be used to evaluate the effects of direct or indirect interaction between crystals during their separation from the melt. These intrusions have a number of advantages: they can be shown to have formed by a single intrusion event, and the origin of the crystals and conditions at the time of intrusion are well constrained.

We initially focus on crystals within the Nosappumisaki intrusion, which is the thickest and most extensively studied; the crystals can be divided into two types without ambiguity based on the texture and composition: crystals that were already present at the time of intrusion ('phenocrysts') and those grown *in situ* after intrusion. Conditions before the start of crystal redistribution are then estimated by combining information from the adjacent intrusions, which exhibit wide variations in thickness. On the basis of these conditions, plausible transportation mechanisms for a highly concentrated suspension of 'phenocrysts' forming non-reactive solid particles in a magma chamber are determined. Lastly, the role played by direct or indirect crystal–crystal interaction in crystal–melt separation in a magma chamber is discussed.

GEOLOGICAL SETTING

The Nemuro peninsula, where the studied sills are located, is situated in eastern Hokkaido (Fig. 1a), and consists mainly of the late Cretaceous Nemuro Group (Sasa & Hayashi, 1952; Matsumoto, 1970; Kiminami, 1978). The Nemuro Group has a total thickness greater than 3000 m and dips gently to the south (15–20°) with a nearly east–west-trending strike (N70–85°E). It is composed of sandstones, mudstones, alternations of sandstone and mudstone, and volcanic breccias associated with alkaline basaltic lava flows and intrusions (Sasa & Hayashi, 1952; Nagao, 1957; Sasa, 1957; Kiminami, 1978). On the basis of their lithofacies, the sedimentary rocks in the group are inferred to have been deposited in a fore-arc basin of the proto-Kuril subduction system (Kiminami, 1983; Kimura & Tamaki, 1986).

Alkali basaltic (shoshonite) sills of various sizes are intruded into the sedimentary rocks of the Nemuro Group (Fig. 1a). These are classified into three types (Yagi, 1969). Type 1 is very thick, sometimes >60 m in thickness, and is composed of a variety of coarse-grained lithologies ranging from gabbro to monzonite. Type 2 is much thinner, usually 10–30 m in thickness, and occasionally associated with pillow structures inside the sill. Type 3 is totally composed of pillow structures.

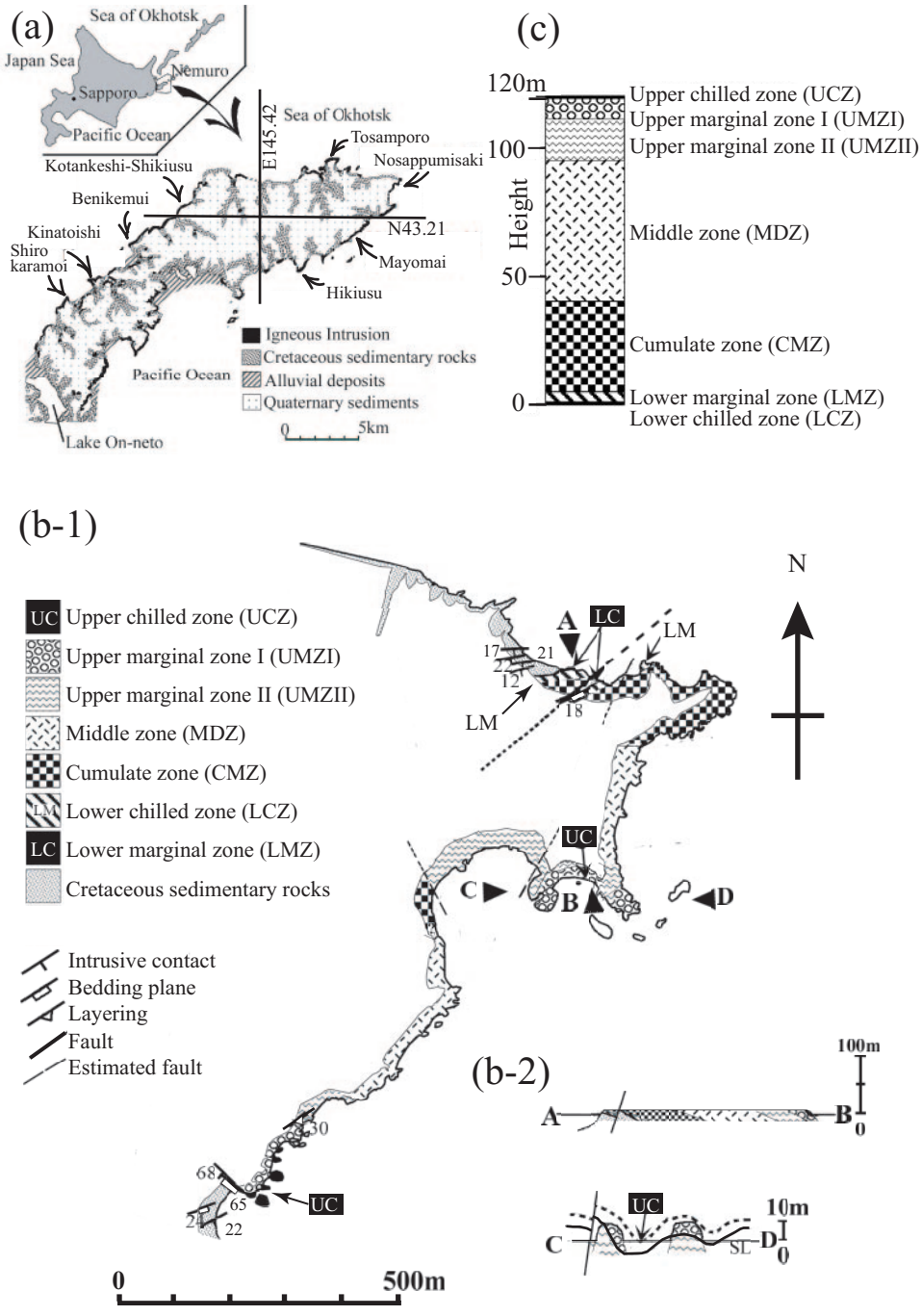

Fig. 1. (a) Simplified geological map of the Nemuro peninsula showing the locations of the studied intrusions: Nosappumisaki, Mayomai, Tosamporo, and Kinatoishi. Other intrusions referred to for their thickness and lithological variations are: Shirokaramoi, Kotankeshi-Shikiusu, and Hikiusu. (b-1) Geological map of the Nosappumisaki intrusion; (b-2) cross-sections through the intrusion. (c) Vertical lithological variation in the Nosappumisaki intrusion.

Paleomagnetic study of these dolerites by Fujiwara & Nagase (1965) clearly indicates a time gap between Type 1 and Types 2 and 3; Type 1 sills always show reversed polarity, but Types 2 and 3 record normal polarity. The association of pillow structures suggests that Types 2 and 3 were either extruded onto or intruded into the Nemuro Group while the sediments were soft and unconsolidated, which is consistent with the ages of the intrusions (Ueda & Aoki, 1968; Shibata, 1985). Type 1 sills have planar intrusion contacts, and are inferred to

have intruded into dewatered and well-consolidated sediments. It is, therefore, concluded that Type 1 intrusions postdate Types 2 and 3 (Fujiwara & Mitani, 1959; Yagi, 1969).

The Nosappumisaki intrusion and other intrusions (Mayomai: ~100 m; Tosamporo: ~80 m; Kinatoishi: ~60 m; Fig 1a) examined in this study belong to Type 1. The Nosappumisaki intrusion is 110–130 m in thickness (Fig. 1b and c) and extends more than 1·5 km. The outcrops are exposed along the shoreline of Cape Nosappu, at the easternmost end of the Nemuro peninsula (Fig. 1a). The lower contact of the sill is parallel to the bedding plane of the Nemuro Group, whereas the upper contact is somewhat irregular with undulations of the order of 10 m (Yagi, 1969) (Fig. 1b). The lower and upper chilled margins are porphyritic with phenocrysts of augite, plagioclase, olivine, and magnetite.

ANALYTICAL METHODS

Whole-rock major and trace element contents were determined by X-ray fluorescence (XRF) using a Philips PW-1480 system at the Department of Earth and Planetary Science of the University of Tokyo, according to the analytical procedure described by Kushiro (1994). The major element contents of the groundmasses of the chilled margins were determined on hand-picked groundmass fragments ~125 μm in size. The studied samples are somewhat altered, but the alteration is limited to replacement of olivine by clay minerals.

Mineral compositions were determined by electron probe microanalysis (EPMA), using a JEOL JCMA-733MKII and a JEOL JXA-8900L system, both at the Department of Earth and Planetary Science of the University of Tokyo. The analytical procedures are similar to those given by Nakamura & Kushiro (1970) with the correction procedure of Bence & Albee (1968) for 15 kV measurement and ZAF for 25 kV measurement. Operating conditions were 15 kV accelerating voltage and 12 nA beam current with 10 s counting time for feldspar and biotite or 40 s counting time for clinopyroxene, and 25 kV accelerating voltage and 50 nA beam current with 100 s counting time for Ni and Cr analyses in olivine and magnetite, respectively. Glass beads obtained by fusion of hand-picked fragments were also analyzed with 15 kV accelerating voltage, 12 nA beam current, a beam width of 10 μm, and 10 s counting time. Amounts of dissolution and overgrowth rims of euhedral augite were determined on the basis of Al X-ray maps of the whole area of thin sections. The ferric content of spinel was calculated by assuming spinel stoichiometry. Modal compositions and the size distribution of crystals were determined by area measurement on digital images of thin sections with a resolution of 800 d.p.i.

THE NOSAPPUMISAKI INTRUSION

Lithological, textural, mineralogical, and whole-rock chemical variations in the Nosappumisaki intrusion are presented in this section. The dominant lithological units are a gabbroic zone in the lower part (LMZ and CMZ in Fig. 1c) and a monzonite zone in the central part of the sill (MDZ and UMZ in Fig. 1c). These two zones are distinct in every feature listed above and are in contact with a gradational lithological change over 10 m (Yagi, 1969). Although Yagi (1969) argued that the compositional variation in the Nosappumisaki intrusion was formed through gravitational settling of crystals grown *in situ*, we consider that the crystals concentrated in the cumulate zone had already crystallized before intrusion of the magma, as demonstrated below. They can easily be distinguished from crystals grown *in situ* on the basis of their texture and chemical composition. In this study, crystals formed before the time of intrusion are called 'phenocrysts' irrespective of the matrix texture and grain size. This does not cause confusion because their unequivocal identity can easily be established by comparison with the phenocrysts in the chilled zones.

Main lithological zones

The vertical lithological variation in the sill is shown in Fig. 1c. The sill is divided into seven zones mostly according to contrasting modal abundances and microstructures (Fig. 2). These are, in ascending order: lower chilled zone (LCZ), lower marginal zone (LMZ), cumulate zone (CMZ), middle zone (MDZ), upper marginal zone II (UMZ II), upper marginal zone I (UMZ I), and upper chilled zone (UCZ).

The modal abundance and morphology of crystals (augite, plagioclase, olivine, and magnetite) that are euhedral and inferred to have been present before intrusion, and those grown *in situ* (groundmass or interstitial part), vary systematically as shown in Fig. 2. In the upper chilled zone (2–3 m in thickness; Fig. 2a) and in the lower chilled zone (~1 m; Fig. 2 h), phenocrysts of augite, olivine, plagioclase, and magnetite are set in a groundmass composed of magnetite, plagioclase, alkali-feldspar, clinopyroxene, biotite and zeolite of 10 μm average size. The upper marginal zone I (~8 m; Fig. 2b) and the lower marginal zone (~4 m; Fig. 2 g) are porphyritic with the same phenocryst assemblage as the chilled zones, but their groundmass is coarser (0·1–0·2 mm average size) than that of the chilled zones. These marginal zones and the chilled zones also differ in their phenocryst abundance of plagioclase and augite (compare Fig. 2 h and g, and Fig. 2a and b). The upper marginal zone II (~14 m; Fig. 2c) is transitional between the upper marginal zone I and the middle zone. The boundary with upper marginal zone I is marked by a sharp decrease in the abundance of plagioclase

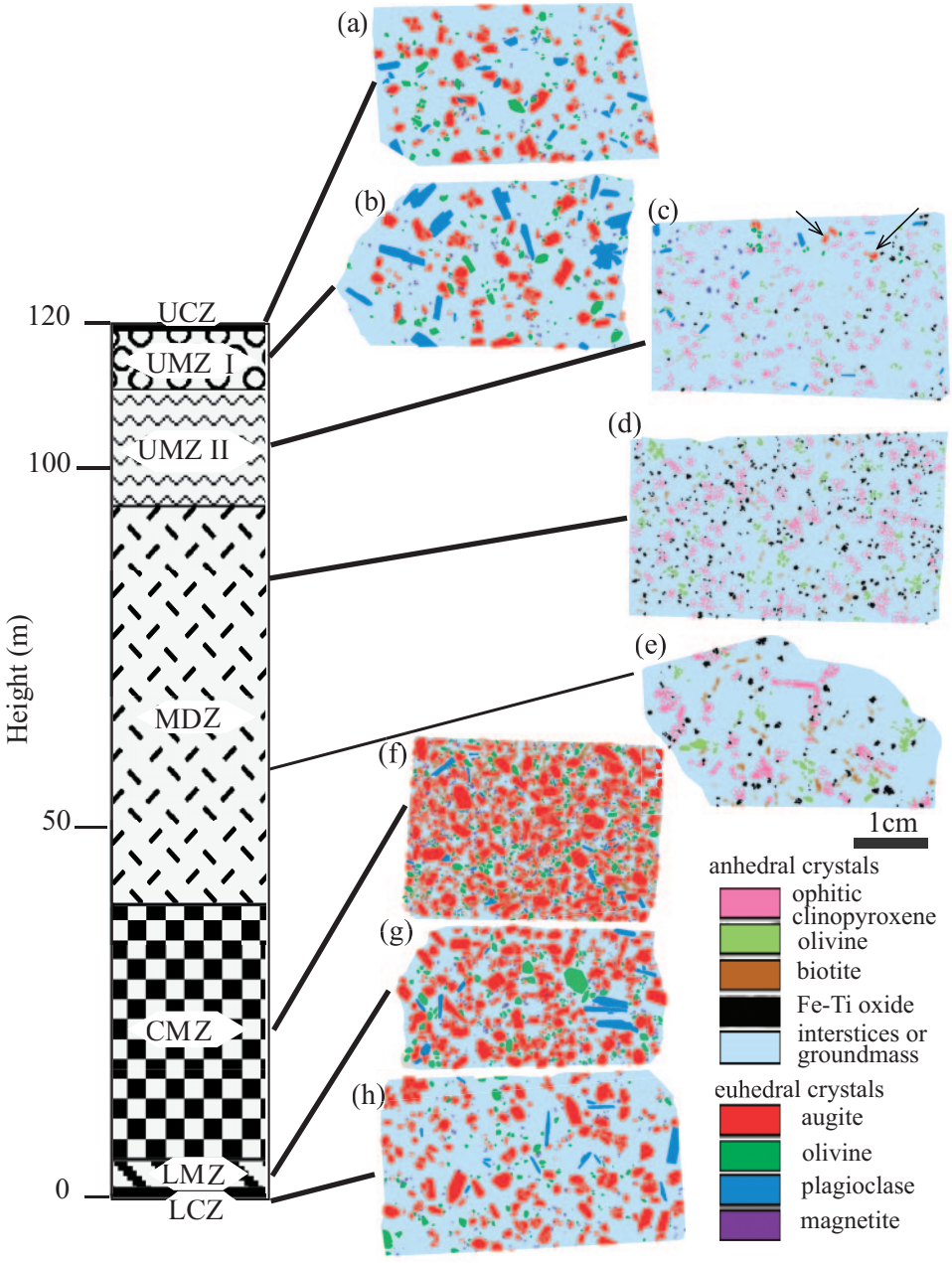

Fig. 2. Representative thin-section drawings for each zone (a–h), showing modal abundance, morphology, and size of the main constituent minerals in the Nosappumisaki intrusion. The color coding is explained in the key: euhedral augite, plagioclase, olivine, and magnetite occur in the lower and upper chilled zones (h, LCZ; a, UCZ), the upper and lower marginal zones (b, UMZ I; g, LMZ), and the cumulate zone (f, CMZ); anhedral clinopyroxene, biotite, magnetite, and olivine occur in upper marginal zone II and the middle zone (c, UMZ II; d and e, MDZ). Arrows in (c) indicate euhedral augite crystals surrounded by ophitic margins. The remaining area represents the interstitial part or groundmass, consisting mostly of alkali-feldspar, Fe-rich fine-grained clinopyroxene, zeolite, and apatite. The scale bar is common for all the thin-section drawings.

'phenocrysts' and that with the middle zone by the disappearance of 'phenocrysts'. The UMZ II is characterized by the occurrence of small euhedral crystals (augite indicated with arrows in Fig. 2c) and weakly developed ophitic texture of clinopyroxene (pink in Fig. 2c) and plagioclase. The cumulate zone (~35 m; Fig. 2f) contains abundant euhedral augite. Lesser amounts of euhedral olivine, plagioclase, and magnetite are also present. These crystals are identified as cumulus phases. Biotite, alkali-feldspar, and zeolite are intercumulus phases and are inferred to have crystallized *in situ*. Zeolite minerals present in this intrusion are primary

magmatic phases crystallized in the latest stage of solidification as shown below. Discrimination of the two types of minerals will be described and discussed in more detail below. The middle zone (~55 m; Fig. 2d and e) is characterized by well-developed coarse ophitic texture consisting of anhedral clinopyroxene enclosing euhedral–subhedral plagioclase. Olivine, magnetite, biotite, alkali-feldspar, and zeolite are also present in this zone. The MDZ is heterogeneous and has wide variation in grain size and mineral mode. Such variations in a single outcrop are particularly noticeable near the bottom of the middle zone, where the maximum grain size attains 4 cm.

Macro-structures

Various veins, layered structures, lenses, and pipe-like structure are observed in the main lithological zones. Among them, leucocratic pipe-like structures, graded layering, and rhythmic veins provide critical information on attitude of the sill at the time of intrusion and are described below (Fig. 3).

Pipe-like structures

Leucocratic pipe-like structures (Fig. 3a) are distributed in the lower marginal zone and in the lower half of the cumulate zone. They are mostly cylindrical in shape. They range in diameter from 1 to 20 cm, and in length from 10 cm to >1 m. The diameter increases, but the density of pipes per unit area decreases, with height above the lower contact. The orientation of the pipe-like structures is perpendicular to the bedding planes of the host sedimentary rocks (Fig. 3a-1). The leucocratic pipe-like structures are composed mainly of alkali-feldspar and zeolite and include euhedral crystals of augite, olivine, and magnetite, which have the same characteristics as in the host rock. These structures are inferred to have formed by melt focusing as a result of the buoyancy of the melt (Yoshida *et al.*, 1981; Carman, 1994; Goff, 1996; Rogan *et al.*, 1996; Caroff *et al.*, 1997).

Graded layering

Graded layering is present near the boundary of the upper marginal zones I and II (Fig. 3b). The layering is parallel to the bedding plane of the surrounding sedimentary rocks (Fig. 3b-1). The layers consist of the same minerals as are present in the surrounding main lithology, but show local concentration or depletion of phenocrysts. The layering consists usually of several repetitions of normally graded layers, which are 10–40 cm in thickness and are traceable for more than 3 m along the layering plane. The boundary of neighboring graded layers is marked by a sharp change in modal abundance. The total abundance of phenocrysts changes from almost none in the top of the layering to more than 10% toward the bottom (Fig. 3b-3). Size grading of phenocrysts is not obvious. The topmost layer of a set of repeated normally graded layers changes upwards to the host main lithology with gradual increase of the modal abundance of phenocrysts over ~1 m distance, showing reverse grading.

Heterogeneity of the main lithology in terms of the abundance of phenocrysts is also observed in the upper marginal zones, where local regions with no or a lesser amount of phenocrysts than the host rocks are present, usually on a scale of a few centimeters to ~1 m (Fig. 3d). These heterogeneities are usually tabular, with rare branching geometries, and are oriented either nearly parallel to or at a high angle to the graded layering. The boundaries with the main lithology are marked generally by abrupt change in the modal abundance on a scale of less than a few centimeters.

Rhythmic veins

Rhythmic veins, oriented parallel to each other with a regular interval, occur in the lower chilled zone. They are nearly parallel to the bedding plane of the host sedimentary rocks (Fig. 3c). They are composed mostly of zeolite. The thickness, interval, and length of the veins increase with height from the lower chilled contact. Such rhythmic veins are also present in the lower marginal zone, but the thickness and interval are larger than those of the chilled zone, and the intervals are irregular. Rhythmic veins are minor in the upper chilled zone, but distinct ones are present in upper marginal zone I. This type of vein (rhythmic veins near the contact) is often reported from sills and dikes (e.g. Pecora, 1941; Carman *et al.*, 1984; Carman, 1994; Goto, 1996), and they are interpreted as 'segregation veins' formed by cooling contraction. Their orientation is usually parallel to the cooling surface (Goto, 1996), indicating that the basal contact was nearly horizontal at the time of intrusion. This is consistent with the orientations of the pipe-like structures and graded layering.

Mineralogy

Textural and mineralogical characteristics of the main constituent minerals in the Nosappumisaki intrusion are presented below in order to clearly distinguish 'phenocrysts' from crystals grown *in situ*. It will be shown that the 'phenocrysts' in the cumulate zone were neither grown nor dissolved before they settled. Some 'phenocrysts' in a particular horizon of the cumulate zone exhibit minor partial dissolution textures with mineralogical features indicating *in situ* interaction with differentiated melt. Such a texture is absent in 'phenocrysts' from other horizons.

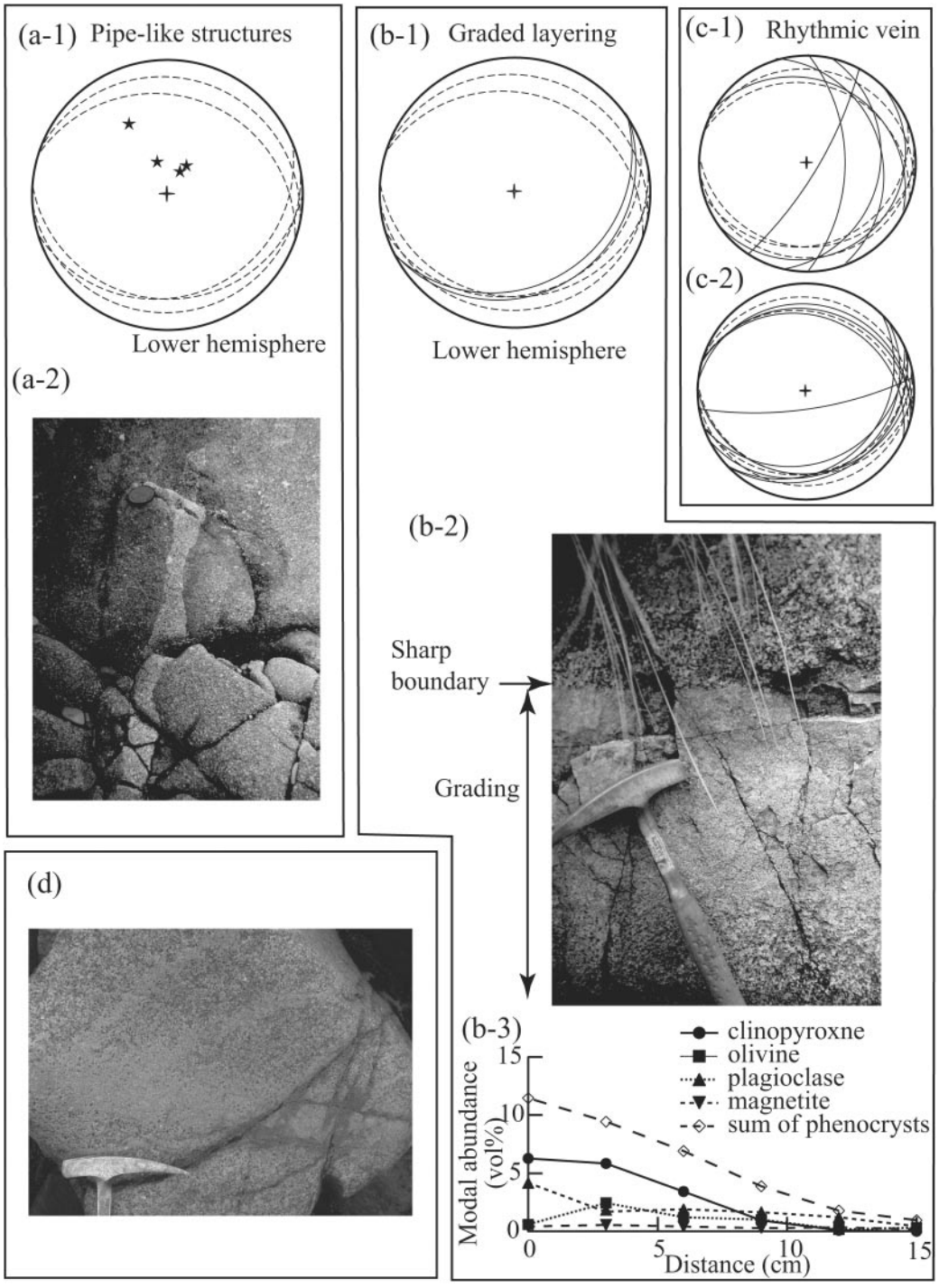

Fig. 3. Pipe-like structure observed in the lower part of the cumulate zone (a), graded layering (b) and modal heterogeneity with rare branching features (d) found near the bottom of upper marginal zone I, and rhythmic veins (c) developed in the chilled zones of the Nosappumisaki intrusion. The orientation of the pipe-like structures in the cumulate zone is shown in (a-1) as stars. The orientation of the graded layering is shown as a continuous line in (b-1). The modal variations in the graded layering are shown in (b-3), in which the distance is measured from the sharp bottom boundary. The orientation of rhythmic veins in the upper chilled zone (c-1) and in the lower chilled zone (c-2) is shown as a continuous line in the stereo plot (lower hemisphere). Dashed great circles in (a-1), (b-1), (c-1), and (c-2) are bedding planes of the surrounding sedimentary rocks. The lens cap in (a-2) is 5 cm across, and the hammerhead in (b-2) and (d) is 25 cm long.

Clinopyroxene

Clinopyroxene occurs either as euhedral crystals, in ophitic texture, or as small subhedral grains (Figs 4 and 5; Table 1). The small subhedral grains are observed in the groundmass of the chilled zones and the marginal zones (Fig. 4). The first two morphological types are distinguishable from each other by their chemical composition (Table 1 and Fig. 6). The chemical composition of euhedral crystals is in the range of 40–43 in Wo [$100 \times Ca/(Mg + Fe + Ca)$] and 12–18 in Fs [$100 \times Fe/(Mg + Fe + Ca)$], whereas ophitic crystals show a large variation ranging from 43 to 47 in Wo and from 13 to 54 in Fs even in a single grain (Fig. 6a). The two types of clinopyroxene are systematically distributed in the sill (Figs 4 and 6b). Euhedral crystals ('phenocrysts') are present in the lower third of the sill (LCZ, LMZ, and CMZ; Fig. 6b) and in the upper quarter (UCZ and UMZ I, II). In contrast, ophitic crystals occur in the central part (MDZ and UMZ II).

Euhedral crystals show oscillatory and sector zoning (Fig. 5a–d), and they commonly include magnetite and olivine. Glass inclusions with trapped vesicles or rounded crystal aggregates after melt inclusions are also observed in euhedral augite throughout the sill. Large aggregates of euhedral augite, with or without other phases (plagioclase, olivine, or magnetite), are sometimes present in the lower third of the sill (LCZ, LMZ, and CMZ) (Fig. 5e). In contrast, ophitic clinopyroxene shows sector zoning but does not have oscillatory zoning. It does not contain any inclusions of magnetite, olivine, or glass (or rounded crystal aggregates). The average chemical composition and zoning pattern of oscillatory and sector zoned augite 'phenocrysts' in the marginal and cumulate zones are the same as that of the chilled zone (Fig. 6), but the morphology and chemical composition of the margins or rims of 'phenocrysts' vary with height in the intrusion (Fig. 4).

In the lower and upper chilled zones, euhedral crystals have straight and regular outlines and show neither dissolution nor overgrowth textures (Fig. 5a). In the lower and upper marginal zones, however, they have overgrowth rims with serrated outlines on a scale of 0·01–0·02 mm and 0·05–0·1 mm, respectively (Figs 4 and 5b). The irregular rims have Fs contents ranging from 20 to 50 (Fig. 4) and are intergrown with small groundmass plagioclase, in a sub-ophitic texture. In the cumulate zone, particularly in the upper half, euhedral crystals have partially dissolved or narrow overgrowth rims, which are 0·1–0·2 mm in width (Figs 4 and 5c). The composition of the partially dissolved rim is Wo44–47 and Fs13–18, and that of the narrow overgrowth rim is Wo43–44 and Fs12–18; these are significantly different from the compositions of the internal part of the crystals (Fig. 6a and Table 1). The width of the partially dissolved rims is very narrow in the lower half of the cumulate zone, and the abundance rapidly increases to ~1 vol. % of the rock towards the top of the zone. The overgrowth rim is thinner than the dissolved rim, and the width increases slightly with height.

There are small, equant, euhedral–subhedral clinopyroxene crystals with oscillatory and sector-zoned cores in the bottom of the middle zone, ~5 m above the cumulate zone. Their core compositions are almost the same as the euhedral augite phenocrysts in the chilled zones (Fig. 4). The modal abundance of clinopyroxene identified as 'phenocrysts' in the lowermost part of the middle zone is <0·05 vol. %. This type of clinopyroxene is restricted to near the bottom of the middle zone.

In the middle zone, anhedral clinopyroxene with an ophitic texture exhibits a remarkable variation in Fs contents (Fig. 6). Each grain of ophitic clinopyroxene shows strong zoning characterized by Fe enrichment and Al depletion from core to rim (Fig. 5f). The most Fe-rich rim attains the composition of Wo45–46 and Fs52. The size of the ophitic clinopyroxene is more than 5 mm near the boundary of the middle zone and the cumulate zone, but is around 2 mm in most of the middle zone (Fig. 2c–e). In upper marginal zone II, which is transitional between the middle zone and upper marginal zone I, euhedral augite phenocrysts enclosed in thick ophitic rims, more than 0·2 mm in width (Fig. 5d), and isolated ophitic clinopyroxenes 0·2–0·5 mm across, coexist (Fig. 2c).

Olivine

Olivine is present throughout the sill (Fig. 2) and is divided into two types according to its morphology. The first type is euhedral and is present in the lower and upper chilled zones, the marginal zones, and the cumulate zone. Euhedral phenocrysts in the upper and lower chilled zones have very straight outlines. Euhedral crystals in the cumulate zone tend to be surrounded by biotite. The second type comprises olivine aggregates or skeletal grains in the middle zone.

Olivine crystals are mostly altered to clay minerals; however, fresh isolated olivine grains occur occasionally in upper marginal zone II, of which the average composition is listed in Table 2. The chemical composition ranges from Fo79 [$Fo = 100 \times Mg/(Mg + Fe)$], NiO 0·08 wt %, and CaO 0·32 wt % in the core to Fo77, NiO 0·06 wt %, and CaO 0·28 wt % in the rim. Olivine also appears as inclusions in augite 'phenocrysts' in the chilled zones, the marginal zones, and the cumulate zone.

Plagioclase

Plagioclase is present in all rock types in the sill, and usually occurs as euhedral crystals; it can be classified

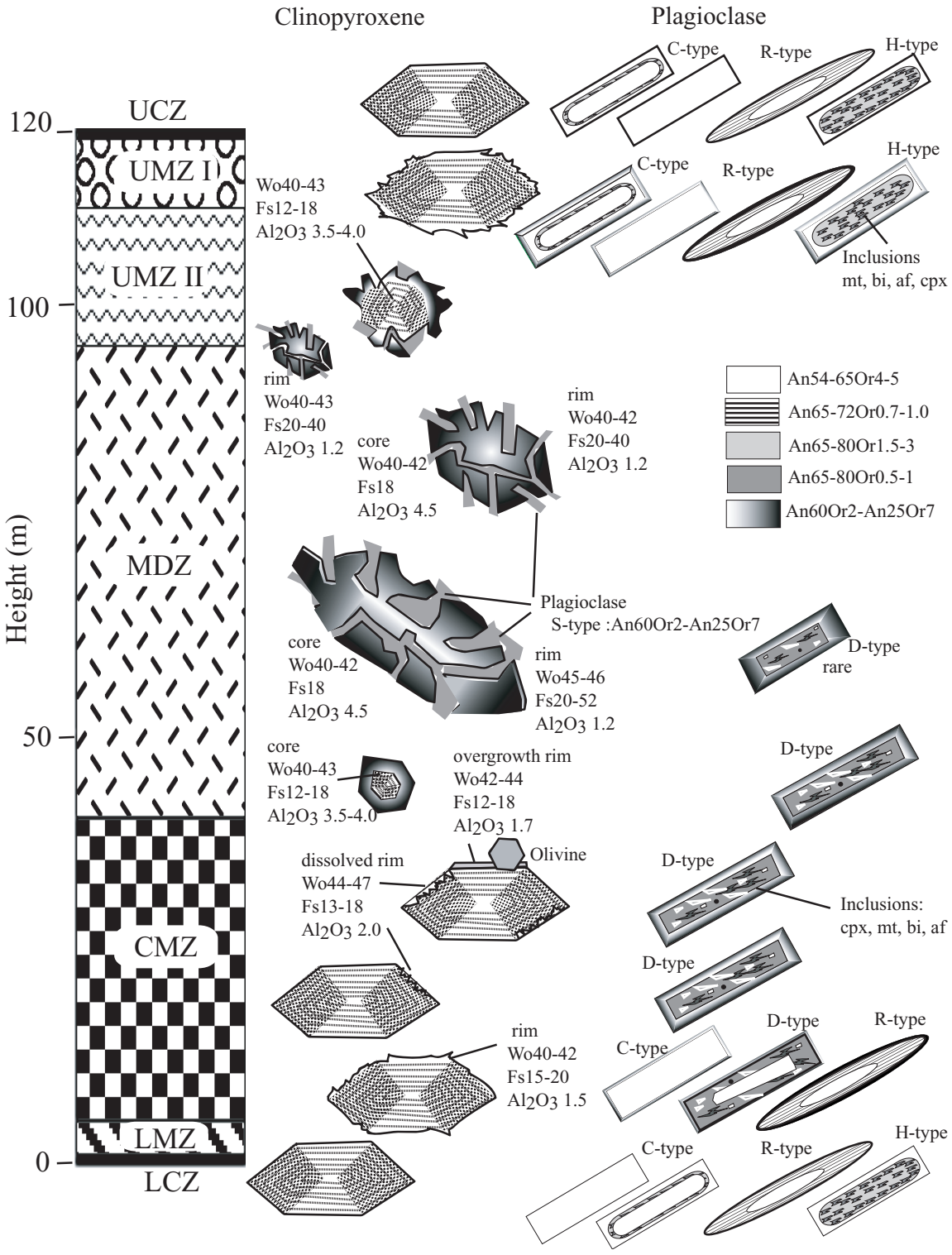

Fig. 4. Schematic diagram showing the chemical composition, morphology, and zoning of clinopyroxene and plagioclase for each lithological zone in the Nosappumisaki intrusion. Striped lines with partial shading in clinopyroxene indicate oscillatory zoning and sector zoning, which is in the range of 40–43 in Wo, 12–18 in Fs, and 3·5–4·0 wt % in Al_2O_3 content. Concentric gradation in clinopyroxene shows monotonous and strong zoning. The range of Al_2O_3 wt %, Wo, and Fs mol % in clinopyroxene are given for each drawing. Plagioclase is classified into five types (C-, R-, H-, D-, and S-type), which are symbolized by schematic drawings. (See text for more details of the classification.) Patterns for plagioclase indicate An and Or contents as shown in the legend.

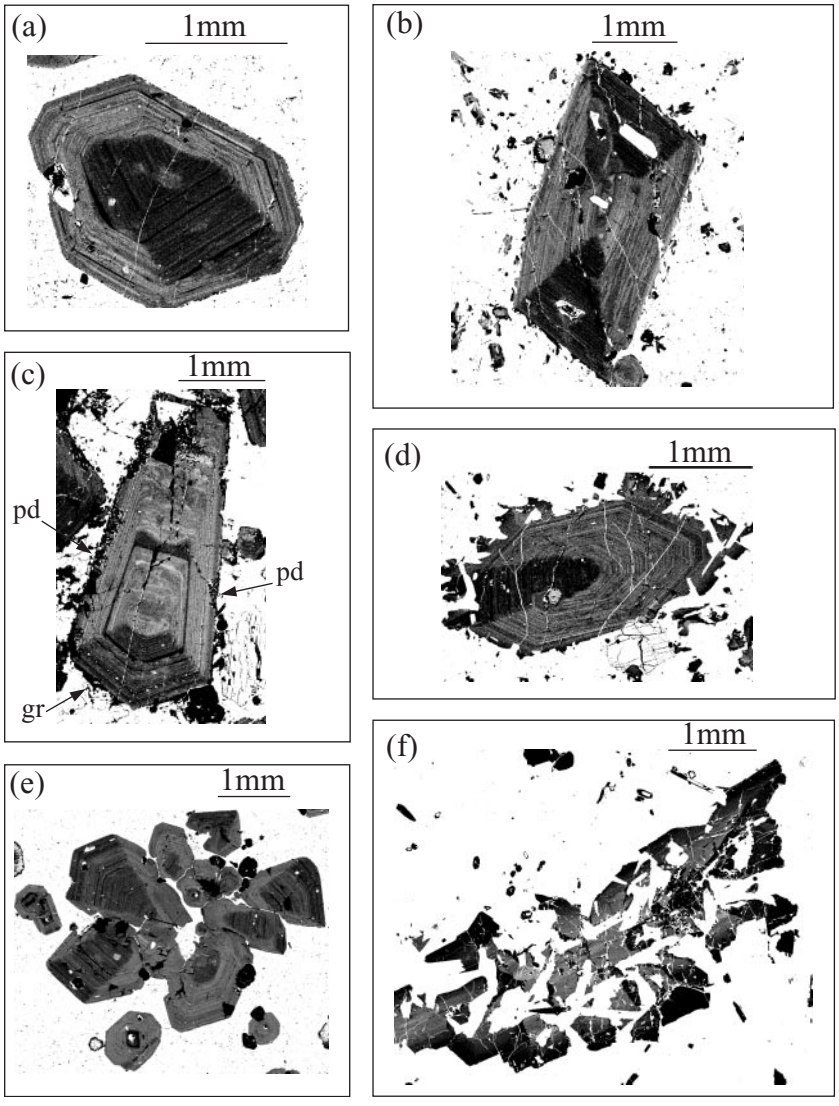

Fig. 5. Gray-scale Al distribution maps for clinopyroxene from different lithological zones of the Nosapppumisaki intrusion. The Al content is higher with increasing brightness. (a) Euhedral augite (phenocryst) with well-formed outline in the chilled zones. (b) Euhedral augite (phenocryst) with irregular and serrated rim from marginal zone I. (c) Euhedral augite crystal having both thin partially dissolved rim (pd) and a thin growth rim (gr) in the middle of the cumulate zone. (d) Euhedral augite surrounded by ophitic texture in upper marginal zone II. (e) Aggregate of euhedral augite in the lower marginal zone. (f) Anhedral clinopyroxene showing sector zoning and ophitic texture with plagioclase in the middle zone. Euhedral augite exhibits oscillatory and sector zoning, as shown in (a)–(e). Oscillatory zoning is absent in ophitic clinopyroxene as shown in (f) and the margin of (d).

into five types according to its texture (Figs 4 and 7) and chemical composition (Fig. 8, Table 3). The first type (Clear; C-type) is characterized by rectangular shapes and a homogeneous composition of An54–65 Or4–5 with weak oscillatory zoning (Figs 7a and 8a). This type has the same compositional range irrespective of horizon in the sill and is characterized by a high K_2O content. The second type (Rounded, R-type) has a rounded shape and a fine dissolution texture in the margin (Fig. 7c), which has a composition An65–72 Or0·7–1·0 (Fig. 8a). This type commonly has a core with the same composition as that of C-type.

The third type (Honeycomb; H-type) is characterized by a honeycomb texture (Fig. 7b). Many melt inclusions, which now consist of crystal aggregates, are distributed in the homogeneous or concentrically zoned core region, which has a composition An65–80 Or1·5–3 (Fig. 8a). The An content does not show local heterogeneity controlled by the presence of 'melt inclusions'. The crystal aggregates in the honeycomb texture consist mainly of magnetite and biotite with subordinate

Table 1: Average chemical compositions of clinopyroxene from each lithological zone

	Lower chilled zone	Lower marginal zone	Cumulate zone			Middle zone			Upper marginal zone			Upper chilled zone
									II		I	
	eu.	eu.	eu.	dis.	gr.	ophitic		eq.	eu.	s.g.	eu.	eu.
						core	rim					
wt %												
SiO_2	50·60	50·40	50·90	52·30	52·80	49·40	50·80	51·10	50·70	50·50	50·90	50·80
Al_2O_3	3·89	3·93	3·66	1·94	1·77	4·50	1·25	3·56	3·29	4·20	3·55	3·60
TiO_2	0·63	0·61	0·55	0·24	0·31	0·83	0·23	0·70	0·75	0·83	0·64	0·51
FeO	7·62	7·59	7·52	7·65	5·88	8·65	15·69	7·38	9·77	7·50	7·99	7·15
MnO	0·21	0·21	0·23	0·30	0·28	0·27	1·01	0·32	0·45	0·31	0·27	0·18
MgO	14·40	14·40	14·30	13·90	14·70	13·70	8·00	14·00	12·70	14·90	14·10	14·80
CaO	22·10	22·30	22·20	22·80	23·70	22·00	22·30	22·40	21·70	22·10	22·00	22·40
Na_2O	0·46	0·45	0·48	0·81	0·53	0·45	0·65	0·45	0·57	0·46	0·45	0·41
K_2O	0·01	0·01	0·01	0·02	0·01	0·02	0·01	0·02	0·01	0·01	0·01	0·01
Cr_2O_3	0·04	0·05	0·05	0·03	0·01	0·01	0·01	0·01	0·01	0·01	0·02	0·15
V_2O_3	0·03	0·05	0·03	0·04	0·01	0·05	0·01	0·05	0·02	0·07	0·03	0·05
NiO	0·02	0·02	0·02	0·02	0·01	0·00	0·03	0·01	0·01	0·01	0·01	0·03

See Figs 4 and 5 for clinopyroxene types. eu., euhedral core; dis., partially dissolved rim; gr., overgrowth rim; eq., equant grains; s.g., small subhedral grains.

amounts of alkali-feldspar and clinopyroxene. The honeycomb region is surrounded by an inclusion-free rim of An54–65 Or4–5 (Figs 7b and 8a). These three types, except for those in the chilled zones, are surrounded by a thin rim zoned from An60 Or1·5 inside to An25 Or7 at the outermost rim (Fig. 4).

The fourth type (Dissolution; D-type) is characterized by a partially dissolved heterogeneous core of An65–80 Or0·5–1·0. It has a strongly zoned rim from An60 Or1·5 inside to An25 Or7 at the outermost rim (Figs 4, 7d, 7e and 8a). The rims tend to be thick along boundaries with interstitial phases (Fig. 7d). The dissolution texture is composed of alkali-feldspar, clinopyroxene, magnetite, and biotite. D-type plagioclase sometimes has a clear core with the same composition as C-type (Fig. 7e). Although the textural appearance of D-type is similar to that of H-type, the presence of significant amounts of clinopyroxene and alkali-feldspar and remarkable An enrichment near the 'melt inclusions' are notable differences from H-type. D-type does not have a clear margin, which is common in H-type.

Small, euhedral plagioclase crystals (<0·5 mm in length), occurring in ophitic texture with clinopyroxene and as isolated grains, form another type of plagioclase (small: S type; Figs 4 and 7f). The composition ranges from An60 Or1·5 to An25 Or7 (Fig. 8a), which is the same as the range for rims of large euhedral plagioclases (C-, R-, H-, and D-types) in the upper and lower marginal zones and the cumulate zone. This type of plagioclase occurs in the groundmass of the chilled (<0·05 mm long) and marginal (0·05–0·01 mm long) zones.

Plagioclase crystals of C-, R- and H-types occur in the lower and upper chilled zones, marginal zone I, and the uppermost part of upper marginal zone II (Fig. 4). D-type plagioclase is restricted to the cumulate zone, and that with the C-type core is restricted to the lower marginal zone. In the middle zone and upper marginal zone II, small plagioclase grains forming ophitic textures (S-type) are present. There is no C-type or R-type plagioclase in the middle zone.

Magnetite

A magnetite–ulvöspinel solid solution occurs in the sill (Figs 9 and 10). Ti-poor magnetite is rich in Al_2O_3 and MgO and the solid-solution extends to the $MgAl_2O_4$ spinel end-member (Fig. 10a). The composition of magnetite is listed in Table 4 and the range of vertical variation is plotted in Fig. 10b.

Magnetite is classified into three types according to its morphology. The first type is termed inclusion type (Inc-type; Fig. 9a), and this occurs as inclusions of 0·1 mm in size in euhedral augite crystals. This type is

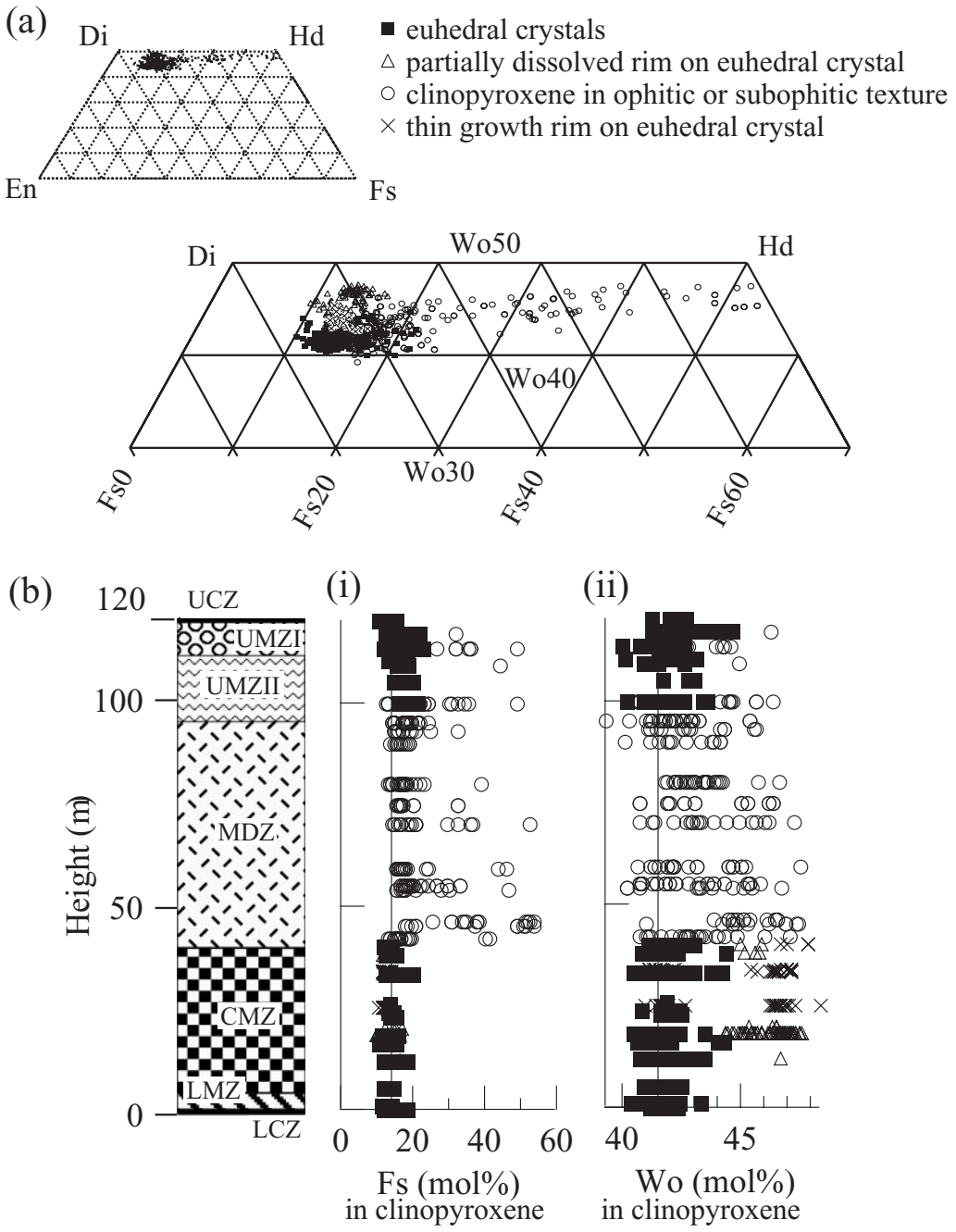

Fig. 6. (a) Chemical composition of clinopyroxene in the Nosappumisaki intrusion projected in part of the pyroxene quadrilateral according to Lindsley (1983). (b) Vertical variation of clinopyroxene composition: ferrosilite mol % (Fs) (i); wollastonite mol % (Wo) (ii).

richest in Cr_2O_3 (∼0·5 wt %), Al_2O_3 (2–3 wt %) and MgO (∼10 wt %) (Table 4 and Fig. 10b). The second type occurs as isolated grains, ∼0·5 mm in size, with a euhedral to subhedral morphology (euhedral–subhedral or E-type; Fig. 9b). This is relatively rich in Cr_2O_3 (0·1–0·5 wt %), and intermediate in Al_2O_3 (∼1·5 wt %) and MgO (∼4·5 wt %). It occurs in the lower and the upper chilled zones and marginal zones as well as in the cumulate zone. The third type is a skeletal type (Skel-type; Fig. 9c), which is characterized by a skeletal morphology and ulvöspinel-rich composition. This type is common in upper marginal zone II and the middle zone. Its size is around 1 mm, and it is poor in Cr_2O_3 (<0·1 wt %), Al_2O_3 (∼1 wt %), and MgO (∼0·6 wt %).

Table 2: Representative chemical composition of olivine from two lithological zones

	UMZ II 'phenocrysts'		CMZ inclusion in augite
	core	rim	
wt %			
SiO_2	37·3	39·1	37·7
NiO	0·09	0·06	0·08
CaO	0·34	0·27	0·23
FeO	22·7	20·9	21·2
MgO	39·9	39·7	39·8

UMZ II, upper marginal zone II; CMZ, cumulate zone.

Skel-type also occurs in the upper marginal zones in the groundmass.

Interstitial minerals

Biotite, alkali-feldspar and zeolite are present in most of the interstices except for those in the chilled zones. They are inferred to have crystallized at a later stage filling the interstitial space between the euhedral crystals because of their absence as phenocrysts in the chilled zone. Biotite is euhedral to subhedral and its size increases from the upper and lower marginal zones to the boundary between the cumulate and the middle zones, followed by a decrease to the bottom.

The morphologies of alkali-feldspar are either euhedral or anhedral throughout the sill. The size ranges from 1 to 3 mm and becomes larger from the upper and lower marginal zones to the boundary between the cumulate and middle zones. Small, subhedral alkali-feldspar is present in the lower and the upper marginal zones, and subhedral to anhedral alkali-feldspar of medium to large size (~2·5 mm) is present in the middle zone and in upper marginal zone II.

Zeolite minerals (analcite, thomsonite, or natrolite) are anhedral, and occur filling interstitial spaces between the other minerals, forming intergrowths with euhedral alkali-feldspar, often including many tiny euhedral apatite crystals. Their occurrence indicates that alkali-feldspar, apatite, and zeolite crystallized in the latest stage of magmatic solidification. Zeolite, which is more abundant in the central part of the sill than in the chilled zones, is not an alteration product of glass, because slow cooling of the central part did not allow glass formation but promoted crystallization of low-temperature minerals directly from the interstitial alkali- and H_2O-rich melt or magmatic fluid. Zeolite minerals are the main constituents in rhythmic veins and leucocratic veins, consistent with their latest crystallization.

Modal abundances

In all the lithological zones of the sill, euhedral crystals of augite, olivine, plagioclase, and magnetite can be easily identified as 'phenocrysts' in the chilled zones on the basis of their morphological and chemical characteristics as described in previous sections. The vertical variation in modal abundance of 'phenocrysts' in the sill is shown in Fig. 11, and the average abundance for each lithological zone is listed in Table 5.

In the lower chilled zone, the augite abundance is 19 vol. %. This rapidly increases to 39 vol. % in the lower marginal zone, and gradually increases to ~40 vol. % through the cumulate zone (Fig. 11a). The olivine abundance is 2 vol. % in the lower chilled zone (Fig. 11b). It dramatically increases to 7 vol. % in the lower marginal zone, and then gradually decreases with height to 5 vol. % in the upper half of the cumulate zone. The plagioclase abundance slightly increases from the lower chilled zone from 2 to 4 vol. % with height and then tends to decrease to 2 vol. % towards the upper part of the cumulate zone (Fig. 11c). Plagioclase is very abundant in the lowermost middle zone just above the cumulate zone (3–8 vol. %). The magnetite abundance shows a variation pattern similar to that of augite (Fig. 11d).

In the upper chilled zone, the augite abundance is 14 vol. %; this rapidly decreases to 0 vol. % in the middle zone through upper marginal zones I (~5 vol. %) and II (2–3 vol. %). The plagioclase abundance is 4 vol. % in the upper chilled zone and increases rapidly downwards, reaching 16 vol. % in upper marginal zone I. The abundance of plagioclase decreases to almost 0 vol. % through upper marginal zone II (~1 vol. %) and finally attains almost 0 vol. % in the middle zone. The olivine abundance is constant at 1·5 % in upper marginal zone I and decreases downwards in upper marginal zone II, attaining 0 vol. % in the middle zone. The magnetite abundance is ~0·5 vol. % in upper marginal zone I. Magnetite slightly increases in abundance in the upper part of upper marginal zone II and decreases downwards to 0 vol. % in the middle zone. The upper marginal zone is also heterogeneous in terms of phenocryst abundance, and phenocryst-free regions are locally present (Fig. 3d), one of which is the graded layering described above (Fig. 3b). In the middle zone, the 'phenocryst' abundance is 0 vol. % except for very rare occurrence of plagioclase in the center and a moderate concentration at the bottom of the middle zone.

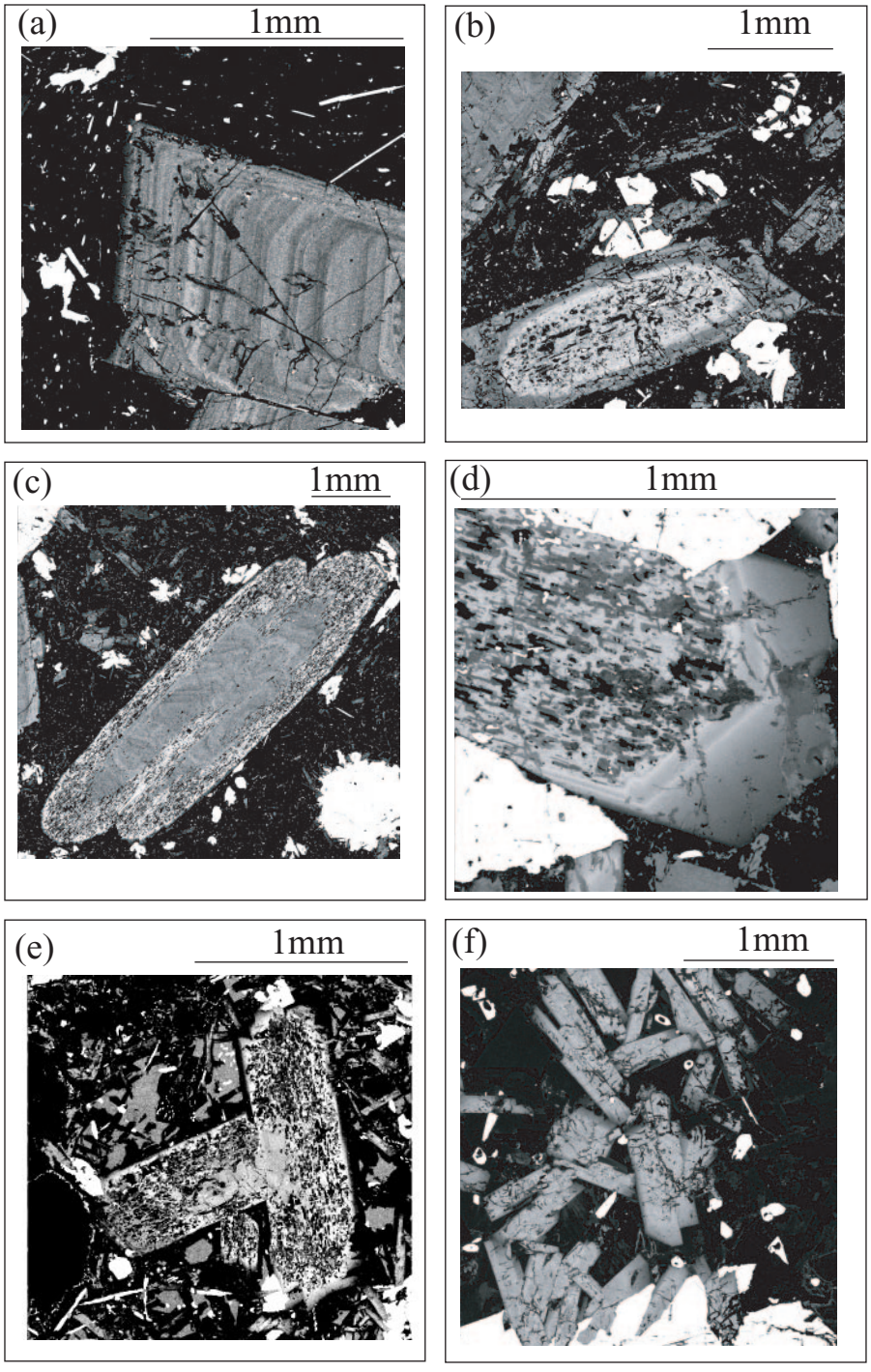

Fig. 7. Gray-scale Ca distribution maps for plagioclase from different lithological zones of the Nosappumisaki intrusion. Darker gray indicates lower, and lighter gray higher Ca contents. (a) Euhedral plagioclase with a very thin Ab-rich rim and oscillatory zoning with average composition of An54–65 Or4–5; (b) plagioclase with a honeycomb core of An65–80 Or1·5–3 and a thick clear rim of An60 Or1 to An25 Or7; (c) rounded plagioclase with a clear core of An54–65 Or4-5 with a finely dissolved margin of An65–72 Or0·7–1; (d) plagioclase with a partially dissolved core of An65–80 Or0·5–1 and a strongly zoned clear rim of An60 Or1 to An25 Or7; (e) same as (d) but with a clear core of An54–65 Or4–5; (f) plagioclase forming ophitic texture with clinopyroxene (near the bottom) and euhedral plagioclase in the interstitial part. (a)–(c) are from upper marginal zone I, (d) and (e) from the cumulate zone, and (f) from the middle zone. Plagioclase types: (a) clear type (C-type); (b) H-type; (c) R-type; (d) and (e) D-type; (f) S-type.

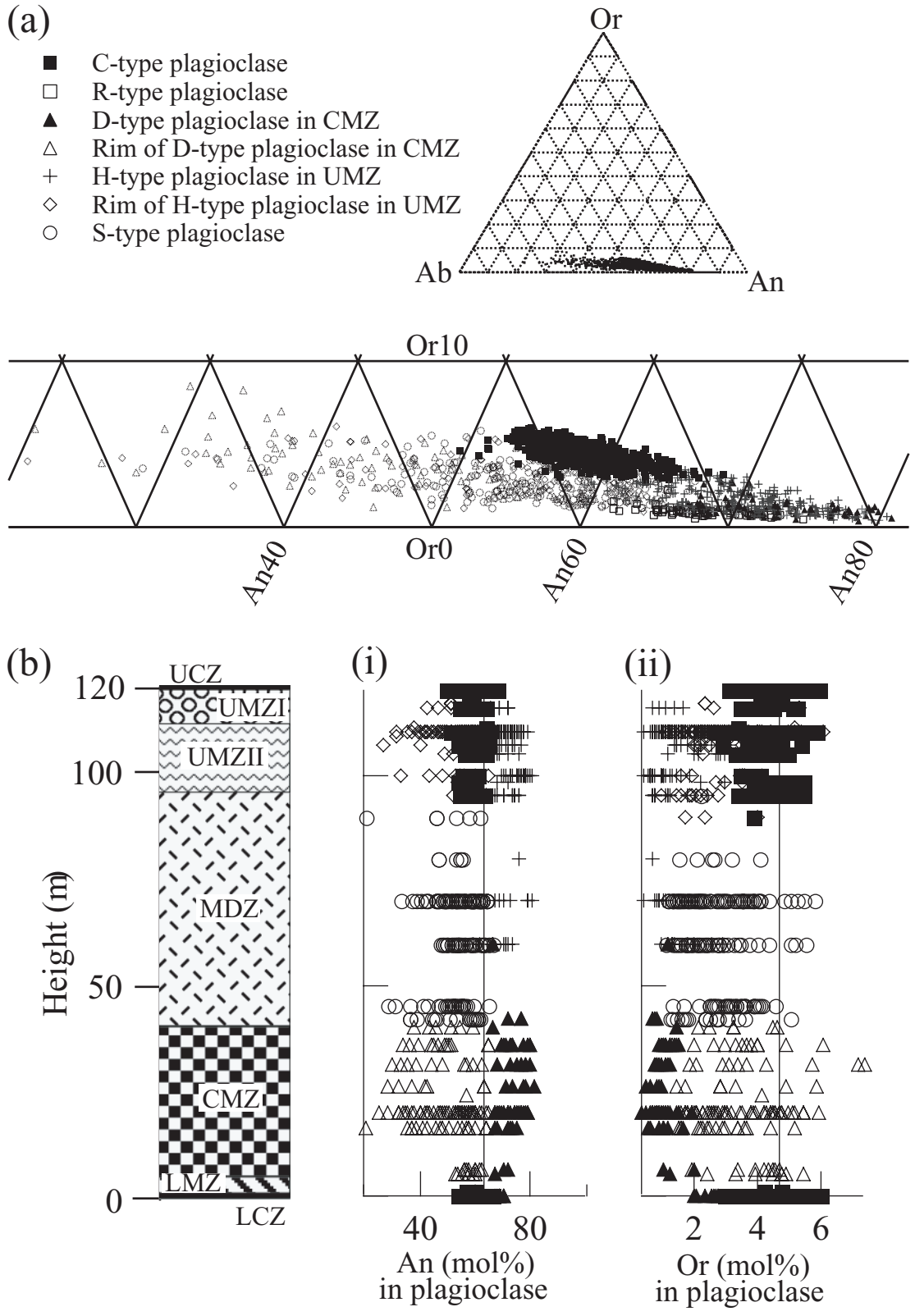

Fig. 8. (a) A part of the orthoclase–albite–anorthite ternary diagram for plagioclase in the Nosappumisaki intrusion. (b) Vertical variation of plagioclase composition: anorthite mol % (An) (i); orthoclase mol % (Or) (ii).

Table 3: Average chemical compositions of plagioclase from each lithological zone

	Lower chilled zone	Lower marginal zone			Cumulate zone		Middle zone	Upper marginal zone II	Upper marginal zone I		Upper chilled zone
Type:	C	R	C	D	D	rim of D	S	C	C	H	C
wt %											
SiO_2	53·3	51·3	52·8	50·7	49·8	55·1	54·4	53·1	53·1	53·0	53·1
Al_2O_3	28·7	30·0	28·5	30·3	31·3	27·7	28·0	28·5	28·6	28·7	28·4
TiO_2	0·05	0·02	0·05	0·02	0·03	0·04	0·05	0·05	0·06	0·06	0·05
FeO	0·84	1·21	0·83	0·89	0·8	0·62	0·7	0·81	0·83	0·79	0·84
MnO	0·02	0·02	0·02	0·01	0·01	0·01	0·02	0·02	0·02	0·01	0·02
MgO	0·1	0·07	0·1	0·04	0·03	0·07	0·06	0·1	0·1	0·09	0·1
CaO	11·8	13·3	11·6	13·6	14·5	10·3	10·8	11·8	11·7	11·8	11·7
Na_2O	4·1	3·37	4·1	3·17	2·95	4·99	4·89	4·13	4·12	4·18	4·19
K_2O	0·76	0·17	0·77	0·28	0·15	0·58	0·46	0·73	0·71	0·42	0·78
Cr_2O_3	0·02	0·01	0·0	0·01	0·02	0·01	0·02	0·02	0·02	0·02	0·02
V_2O_3	0·02	0·02	0·01	0·01	0·01	0·02	0·02	0·02	0·01	0·01	0·02
NiO	0·02	0·01	0·5	0·02	0·05	0·02	0·02	0·02	0·02	0·01	0·02

See Figs 4 and 7 for plagioclase types.

Size distributions

Vertical variations in the size distribution of augite 'phenocrysts' and the average size of 'phenocrysts' are shown in Fig. 12. The average size of augite phenocrysts in the upper chilled zone tends to be smaller than that in the lower chilled zone (Fig. 12a). The difference is mostly attributable to the higher concentration of large augite phenocrysts in the lower chilled zone than in the upper chilled zone, where augite phenocrysts larger than ~3 mm are absent (Fig. 12e).

The average size of augite and magnetite in the cumulate zone is highly variable and does not show any systematic variation with height (Fig. 12a and d). The average size of plagioclase and olivine tends to decrease slightly with height in the cumulate zone, after increasing in the lower marginal zone, although there are many samples with exceptionally smaller sizes (Fig. 12b and c). The size of plagioclase phenocrysts increases from the upper chilled zone to the bottom of upper marginal zone I, from which they decrease towards the boundary of upper marginal zone II and the middle zone. The size of magnetite tends to increase from the top of upper marginal zone I to the bottom of upper marginal zone II. The average size of augite and olivine phenocrysts shows scatter in the upper marginal zones, but tends to increase downwards from the upper chilled zone, followed by a decrease to the top of the middle zone.

In the cumulate and lower marginal zones, most of the cumulative curves shift to the larger grain sizes as compared with the curves for the lower chilled zone (LCZ) (Fig. 12g and h). In contrast, in the upper marginal zones, where phenocrysts are low in abundance, except for plagioclase, the pattern of cumulative curves varies with height (Fig. 12f). Larger augite phenocrysts (2–3 mm in size) become rare in the lower part of the upper marginal zone, where the cumulative curves are notably below the curve for the chilled zone. In contrast, in the upper part of the upper marginal zone, the size distribution is locally similar to that of the cumulate zone. The average aspect ratio of 'phenocrysts' of augite, olivine, and magnetite, measured in thin section, is 0·8 throughout the sill, whereas the aspect ratio of plagioclase ranges from 0·5 to 0·7.

Whole-rock compositions

Average whole-rock chemical compositions of each zone are listed in Table 6, and nine major oxides are plotted against stratigraphic height in Fig. 13. The overall variations are S-shaped or flipped S-shaped as reported from other sills (Hurlbut, 1937; Wilshire, 1967). Below the boundary between the cumulate zone and the middle zone (CM boundary), the contents of TiO_2, FeO, MnO, MgO, CaO and compatible trace elements are higher than those above the CM boundary, whereas the contents of SiO_2, Al_2O_3, Na_2O, K_2O and

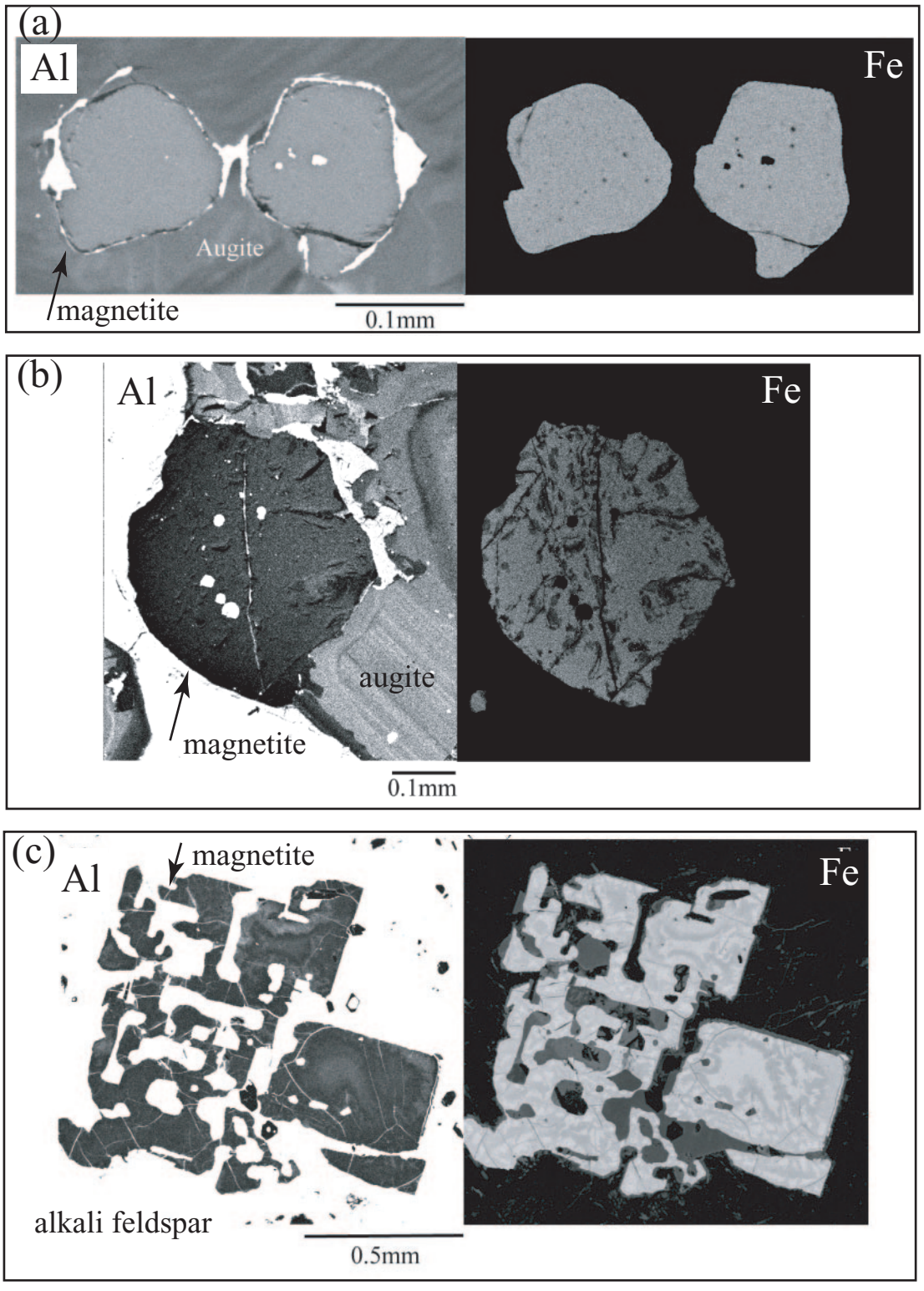

Fig. 9. Gray-scale distribution maps of Al and Fe for magnetite in the Nosappumisaki intrusion. The element contents are higher as the brightness increases. (a) Magnetite inclusions in augite (Inc-type) from the lower chilled zone; (b) euhedral–subhedral magnetite (E-type) from the upper part of the cumulate zone; (c) skeletal magnetite (Skel-type) intergrown with biotite and apatite in the middle zone. Magnetite inclusion is rimmed with aggregate of alkali-feldspar and biotite, white part in the Al map of (a). Subhedral magnetite in (b) shows strong enrichment of Fe and depletion of Al towards the rim in contact with minerals filling the interstices of euhedral crystals.

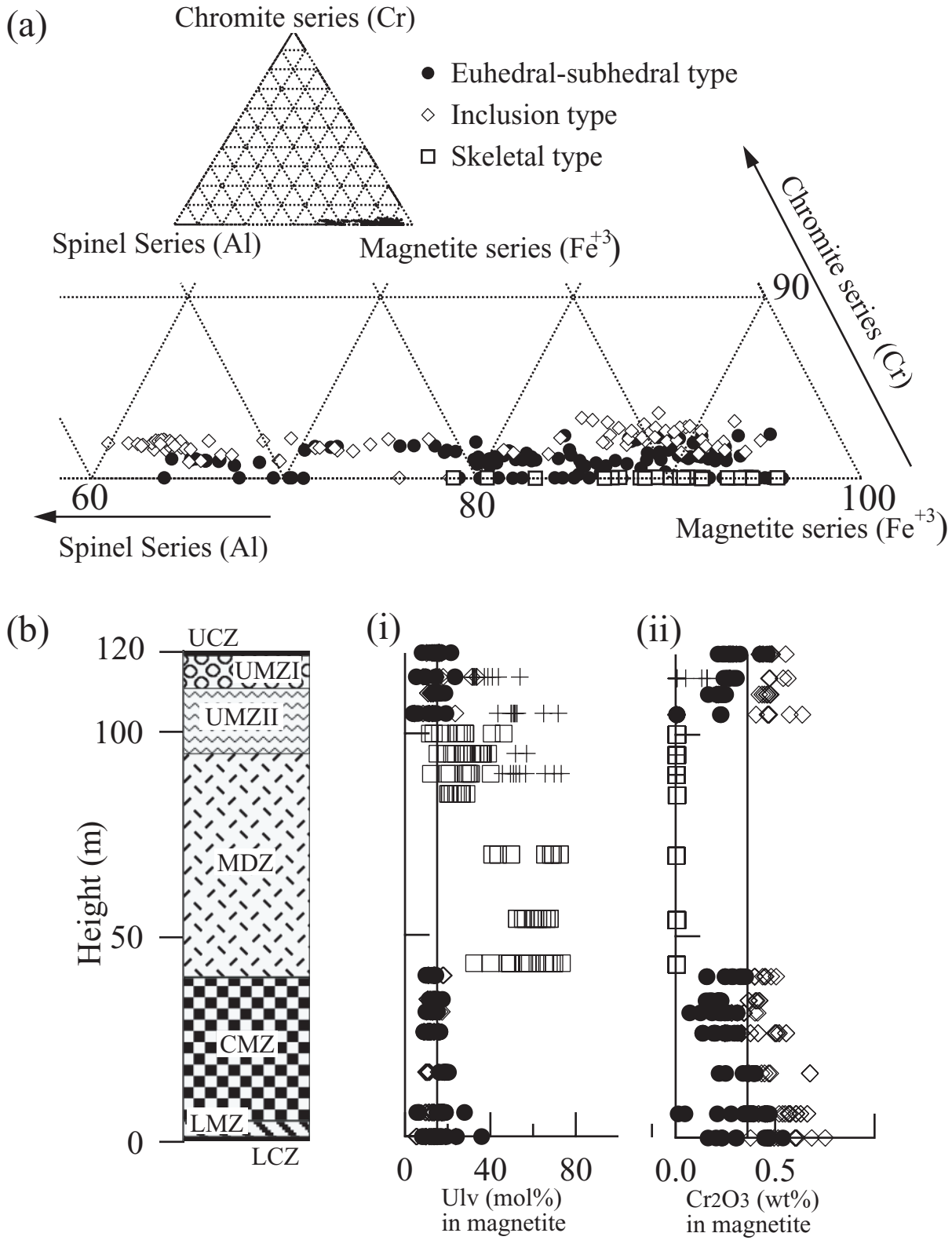

Fig. 10. (a) Chemical composition of magnetite in the Nosappumisaki intrusion plotted in the spinel ternary diagram: Al (spinel series)–Cr (chromite series)–Fe^{3+} (magnetite series). (b) Vertical variation of magnetite composition: ulvöspinel (Ulv) mol % (i); Cr_2O_3 wt % (ii).

Table 4: Average chemical compositions of magnetite cores from each lithological zone

	Lower chilled zone		Lower marginal zone		Cumulate zone		Middle zone	Upper marginal zone II		Upper marginal zone I		Upper chilled zone	
Type:	E	Inc	E	Inc	E	Inc	Skel	E	Inc	E	Inc	E	Inc
wt %													
Al_2O_3	1·68	2·35	1·34	1·76	2·62	4·35	1·02	3·29	1·50	1·41	1·72	1·14	1·38
TiO_2	8·07	6·21	7·12	6·58	6·91	6·58	15·83	9·95	7·88	8·21	8·79	8·16	7·68
FeO	64·0	59·8	63·8	62·8	62·2	52·7	65·9	58·7	66·1	64·4	62·6	62·1	63·0
MnO	0·95	0·74	0·86	1·17	1·33	1·23	2·27	1·93	1·12	0·94	0·99	4·34	2·34
MgO	4·10	9·02	4·54	5·28	5·57	16·15	0·64	8·64	1·55	3·76	5·76	2·65	3·81
Cr_2O_3	0·36	0·54	0·30	0·50	0·26	0·41	0·00	0·08	0·52	0·12	0·27	0·30	0·40
V_2O_3	0·20	0·17	0·19	0·18	0·23	0·19	0·24	0·25	0·18	0·25	0·23	0·22	0·20

See Fig. 9 and the text for magnetite types.

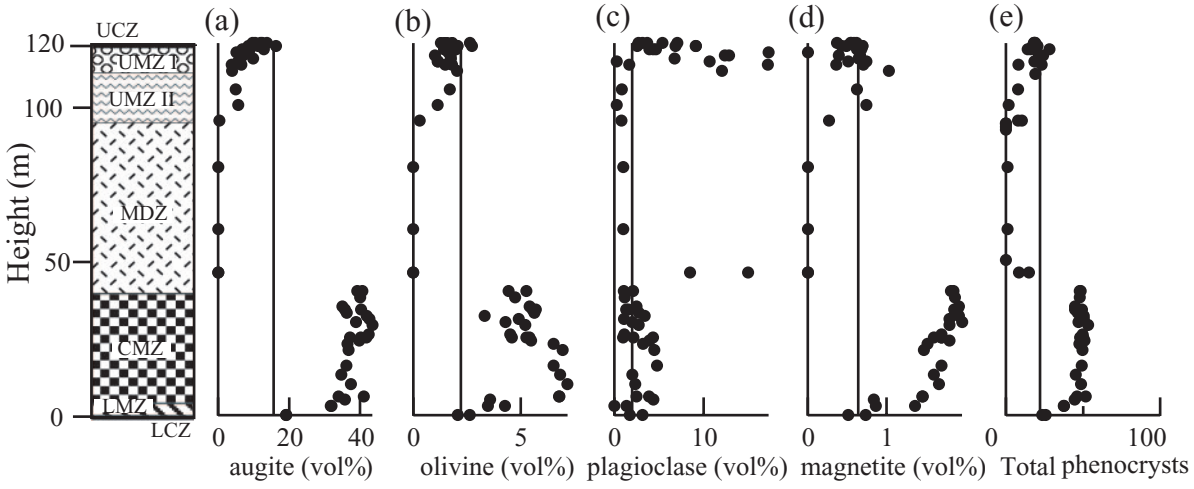

Fig. 11. Vertical variation of the modal abundances of euhedral crystals ('phenocrysts') in the Nosappumisaki intrusion: (a) augite; (b) olivine; (c) plagioclase; (d) magnetite; (e) total 'phenocrysts'. Vertical lines represent the average modal abundance of the upper and lower chilled zones.

incompatible trace elements in the lower half below the boundary are lower than those above. The most felsic and fractionated part of the sill is located 10 m above the CM boundary (~50 m from the bottom).

Other intrusions in the Nemuro Peninsula

The petrological variation of three further intrusions in the Nemuro Peninsula, the Mayomai, Tosamporo, and Kinatoishi intrusions (Fig. 1 and 14a), provide crucial information to constrain the time-scale of 'phenocryst' redistribution relative to the solidification time of the Nosappumisaki intrusion. These are much thinner than the Nosappumisaki intrusion, ranging from 100 m to 60 m. Their mineralogical and petrographic characteristics, as well as the whole-rock composition of the chilled margins (Table 6), are very similar to those of the Nosappumisaki intrusion, but their 'phenocryst' distributions are intimately related to the thickness of the intrusion. All three intrusions contain both 'phenocrysts' (augite, plagioclase, olivine, and magnetite) and crystals grown *in situ* (alkali-feldspar, biotite, zeolite etc.) as in the case of the Nosappumisaki intrusion. Vertical variations in modal abundance in the Mayomai and Tosamporo intrusions show an S-shaped character with 'phenocryst'-accumulated bottom zones and overlying 'phenocryst-free' zones, as in the case of the Nosappumisaki intrusion. In contrast, the Kinatoishi intrusion shows an S-shaped 'phenocryst' distribution, but does not have a 'phenocryst-free' zone overlying the cumulate zone.

Table 5: Average modal abundance (vol. %) in each lithological zone

Zone	augite		olivine		plagioclase		magnetite		Total	Interstitial
	av.	sig.	av.	sig.	av.	sig.	av.	sig.	pheno.	part
UCZ	12·1	2·54	2·06	0·63	4·96	1·57	0·66	0·19	19·8	80·2
UMZ I	8·44	3·62	1·76	0·43	9·27	4·73	0·59	0·23	20·07	79·93
UMZ II (upper)	3·0	0·5	1·2	0·5	2·0	0·5	0·2	0·5	6·4	93·6
UMZ II (lower)	0·0	0·0	0·0	0·0	0·0	0·0	0·0	0·0	0·0	100·0
MDZ	0·0	0·0	0·0	0·0	0·0	0·0	0·0	0·0	0·0	100·0
CMZ (upper)	39·1	2·6	4·93	0·76	1·89	0·79	0·57	0·92	46·5	53·5
CMZ (middle)	39·8	2·73	5·5	0·85	2·87	1·37	0·18	0·52	48·3	51·7
CMZ (lower)	36·1	1·35	6·85	0·32	3·04	1·51	0·55	0·96	46·5	53·5
LMZ	35·1	4·33	6·81	1·56	2·48	1·85	1·45	0·32	45·9	54·1
LCZ	19·2	0·02	2·35	0·39	1·72	1·01	0·62	0·16	23·9	76·1
Av. of CZs	15·7		2·21		3·34		0·64		21·8	78·2

UCZ, upper chilled zone; UMZ I, upper marginal zone I; UMZ II, upper marginal zone II; MDZ, middle zone; CMZ, cumulate zone; LMZ, lower marginal zone; LCZ, lower chilled zone; Av. of CZs, average of the upper and lower chilled margins; pheno., phenocrysts.

The Tosamporo intrusion (Fig. 14a) has a good lateral exposure of the cumulate zone (500–800 m), but does not show any systematic lateral change in the modal abundance of 'phenocrysts'. Correlation between the total height and thickness of the 'phenocryst'-accumulated bottom zone of the intrusions in the Nemuro peninsula is illustrated in Fig. 14b and c.

FORMATION PROCESS OF THE NOSAPPUMISAKI INTRUSION: CONDITIONS AT THE TIME OF INTRUSION

The intrusion process of a sheet-like magma body can be divided into two stages: the earliest stage, during which the magma had the first contact with the surrounding sedimentary rocks by fracture propagation, and a later stage of continuous or intermittent magma supply. Information on the earliest stage must have been frozen in the upper and lower chilled margin rocks because they have a fine-grained or glassy texture, indicating rapid cooling. They would not represent the intruded magma itself if the host rocks had partially melted and these melts were mixed with the intruded magma (Huppert & Sparks, 1989). However, there is no evidence for such an event in the Nosappumisaki and the other studied intrusions. On the basis of the pristine nature of the chilled margins and the textural and compositional equivalence of the phenocrysts in the upper and lower chilled rocks to the euhedral crystals ('phenocrysts') distributed in the studied intrusions, it was concluded in the previous section that such 'phenocrysts' were already present at the time of intrusion. Moreover, the insignificant overgrowth on augite 'phenocrysts' in the cumulate zone, and that on plagioclase 'phenocrysts', with the exception of the rims in contact with the interstitial crystals grown *in situ*, clearly suggests that overgrowth on 'phenocrysts' during crystal settling was fairly limited in the Nosppumisaki intrusion. It is, therefore, concluded that crystal settling was completed in a much shorter time than the cooling of the central zone, permitting us to treat 'phenocrysts' as non-reactive particles during their redistribution process.

In this section, the conditions at the very early stage of intrusion are first estimated from the chilled margin rocks. The 'initial conditions' are critical to reconstruct 'phenocryst' redistribution and solidification processes in the sill. The relevant conditions are temperature, pressure (depth of intrusion and depth of phenocryst crystallization), melt composition including H_2O content, and phenocryst abundances. The depth of phenocryst crystallization may provide additional evidence for the presence of phenocrysts in the intruded magma. Subsequently, the homogeneity of the intruded magma and the style of injection (single or multiple injection) will be examined from the information on 'phenocryst' distribution and observations from the other intrusions in the Nemuro Peninsula.

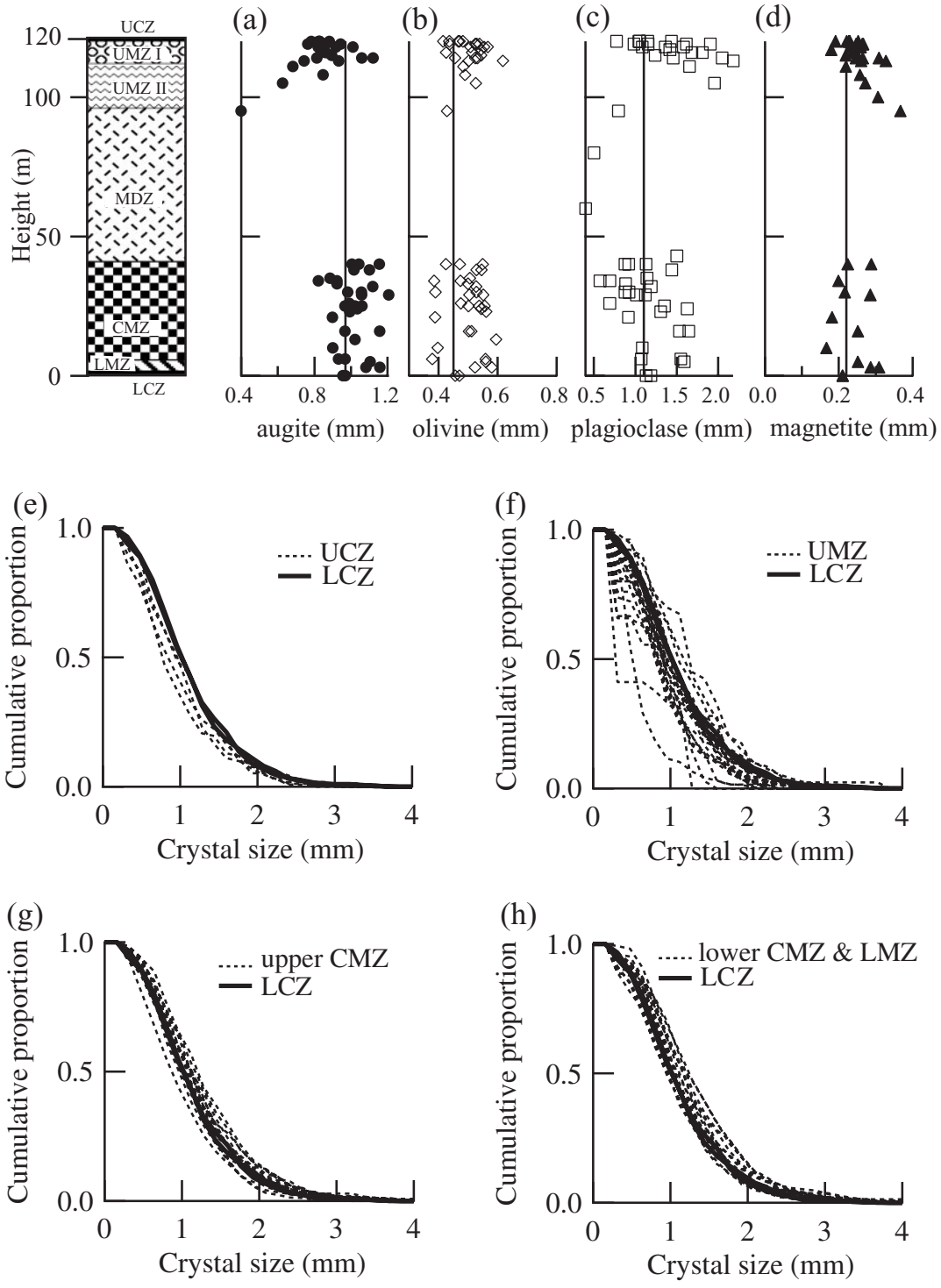

Fig. 12. Vertical variation of the average size of 'phenocrysts' (the average of diameters of circles with the same area for each grain in thin-section drawings) for the Nosappumisaki intrusion in the top panel: (a) augite, (b) olivine, (c) plagioclase, and (d) magnetite. Size measurements were made on 100–500 grains for each mineral except for plagioclase. For plagioclase, 10–50 grains were averaged for the chilled zone, marginal zones, and the cumulate zone, and a few grains for the middle zone. Continuous lines indicate the average sizes in the chilled zones. The cumulative proportion diagrams for the size distribution of augite 'phenocrysts' in each horizon are shown in the lower panels (e) for the upper and lower chilled zones (UCZ and LCZ), (f) for the upper marginal zone I and II (UMZ I and II), (g) for the upper part of the cumulate zone (CMZ), and (h) for the lower part of the cumulate zone (CMZ) and the lower marginal zone (LMZ). The size distribution for the lower chilled zone is shown with bold continuous lines for reference.

Table 6: Average whole-rock composition for each lithological zone of the Nosappumisaki intruson and whole-rock composition of the upper chilled margins of the three studied sills in the Nemuro peninsula

	Lower chilled zone		Lower marginal zone		Cumulate zone (lower)		Cumulate zone (middle)		Cumulate zone (upper)		Middle zone (lower)	
	av. (2)	sig.	av. (10)	sig.	av. (18)	sig.	av. (16)	sig.	av. (29)	sig.	av. (12)	sig.
wt %												
SiO_2	52·0	0·40	50·0	0·43	48·9	0·52	47·8	0·50	47·7	0·52	53·0	1·10
Al_2O_3	14·00	0·55	11·80	0·36	11·00	0·39	10·10	0·24	10·20	0·26	18·80	0·41
TiO_2	0·70	0·00	0·71	0·01	0·71	0·02	0·72	0·02	0·74	0·02	0·74	0·06
FeO	9·78	0·14	10·70	0·34	10·90	0·25	11·40	0·23	11·60	0·30	7·80	0·40
MnO	0·20	0·01	0·22	0·02	0·22	0·02	0·22	0·01	0·22	0·01	0·16	0·02
MgO	8·11	0·35	10·20	0·41	11·20	0·40	12·20	0·20	11·80	0·25	3·75	0·57
CaO	8·20	0·99	11·10	0·43	12·20	0·40	13·30	0·27	13·10	0·45	6·32	1·12
Na_2O	3·65	0·52	3·40	0·63	2·91	0·56	2·34	0·29	2·50	0·28	5·19	0·89
K_2O	3·37	0·25	1·92	0·81	1·99	0·72	2·06	0·39	2·04	0·38	4·26	1·44

	Middle zone (middle)		Middle zone (upper)		Upper marginal zone II		Upper marginal zone I		Upper chilled zone	
	av. (18)	sig.	av. (20)	sig.	av. (16)	sig.	av. (40)	sig.	av. (5)	sig.
wt %										
SiO_2	55·9	1·41	55·0	0·39	54·6	0·51	53·3	0·44	53·1	0·60
Al_2O_3	19·20	0·40	19·00	0·18	19·20	0·43	17·60	1·07	16·10	0·25
TiO_2	0·68	0·06	0·70	0·01	0·65	0·03	0·67	0·03	0·69	0·01
FeO	6·28	0·92	6·81	0·22	6·76	0·29	7·89	0·67	8·61	0·29
MnO	0·15	0·01	0·19	0·03	0·18	0·05	0·19	0·04	0·21	0·02
MgO	2·58	0·51	2·80	0·18	3·07	0·36	4·86	0·91	6·19	0·28
CaO	3·63	1·10	4·10	0·33	4·90	0·81	6·57	0·54	6·65	0·47
Na_2O	5·10	0·51	5·73	0·51	5·48	0·55	4·83	0·49	4·74	0·20
K_2O	6·54	0·75	5·64	0·37	5·16	0·53	4·15	0·61	3·67	0·22

	Upper chilled margin		
	Mayomai	Tosamporo	Kinatoishi
wt %			
SiO_2	53·6	52·7	52·4
Al_2O_3	17·3	15·6	16·1
TiO_2	0·67	0·68	0·61
FeO	7·89	7·96	9·04
MnO	0·22	0·17	0·21
MgO	4·88	8·72	6·99
CaO	6·60	6·89	7·32
Na_2O	4·54	3·27	4·04
K_2O	4·36	3·95	3·26

Number of samples averaged is indicated in parentheses.

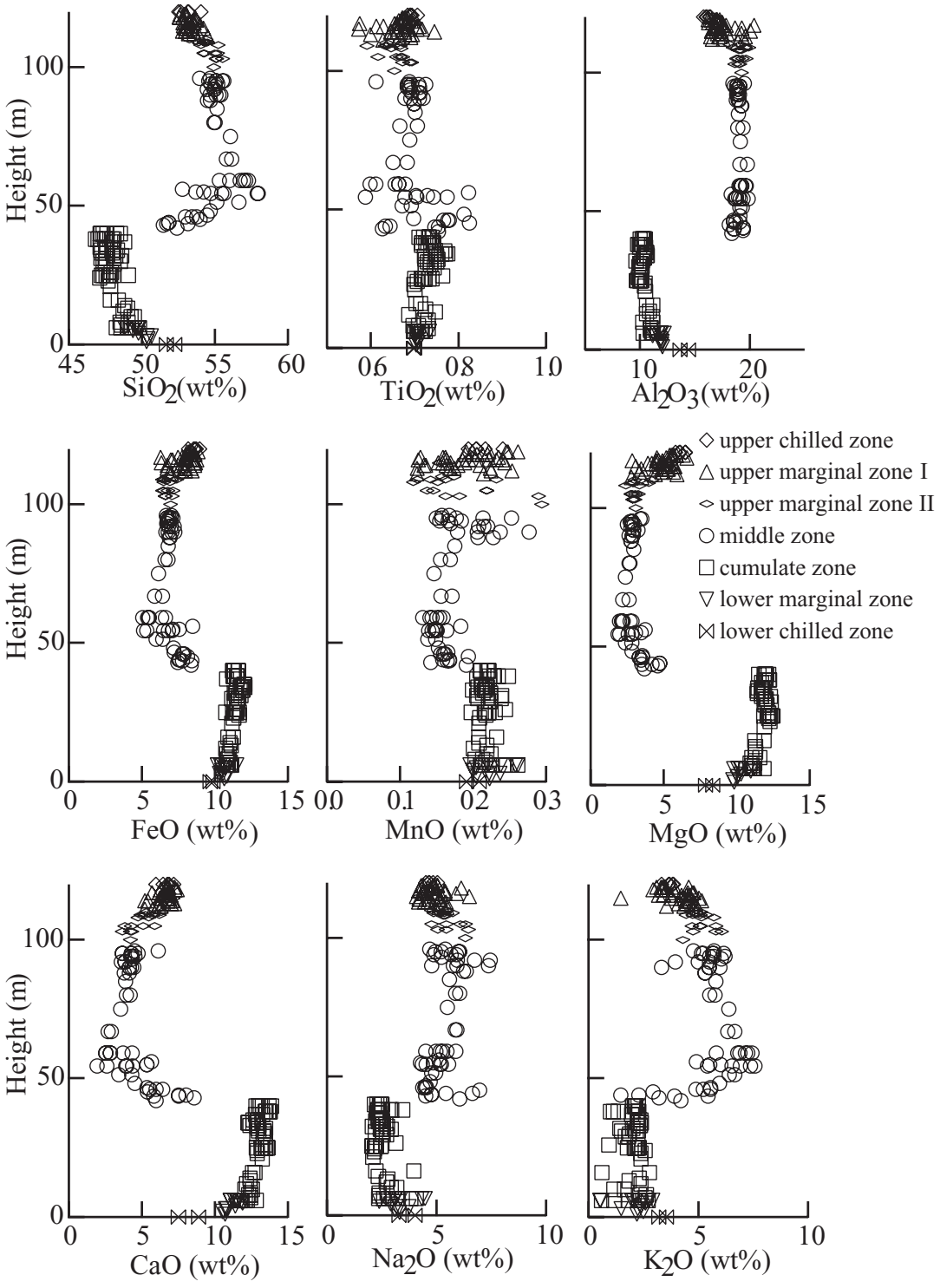

Fig. 13. Vertical variation of whole-rock chemical composition of the main lithologies of the Nosappumisaki intrusion. Major element oxides are recalculated to 100 wt % volatile free.

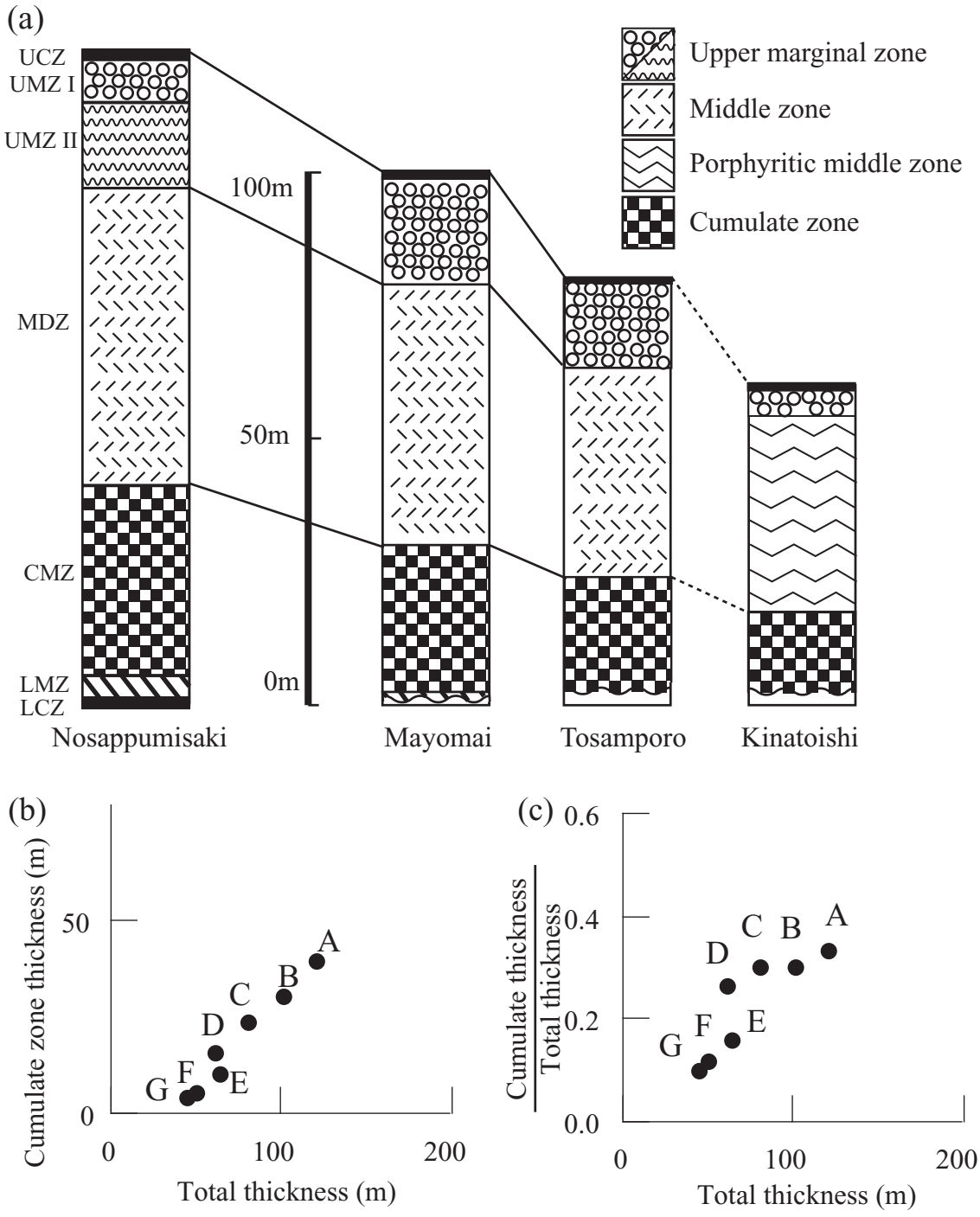

Fig. 14. (a) Reconstructed columnar sections of the Nosappumisaki, Mayomai, Tosamporo, and Kinatoishi intrusions. Porphyritic middle zone represents a leucocratic zone with a porphyritic appearance. Lower chilled margins are not observed in the Mayomai, Tosamporo, and Kinatoishi intrusions, but the thickness of the Mayomai intrusion can be estimated from the host-rock distribution. The thicknesses of the Tosamporo and Kinatoishi intrusions are minimum estimates. (b) Thickness of the cumulate zone and its ratio to the total thickness (c) for the igneous intrusions of the Nemuro peninsula plotted against the total thickness of the intrusion. Data sources are Takahashi (1978) and Matsui & Yoshimoto (1987), except for those shown in (a). Intrusions: A, Nosappumisaki; B, Mayomai; C, Tosamporo; D, Kinatoishi; E, Hikiusu; F, Kotankeshi–Shikiusu; G, Sirokaramoi.

Table 7: Melt composition at the time of intrusion

	Estimated liquid	Groundmass		Groundmass		Calculated groundmass			
		in LCZ EPMA	in UCZ EPMA	in LCZ XRF	in UCZ XRF	LCZ	sig.	UCZ	sig.
wt %									
SiO_2	54·8	54·8	54·7	54·6	55·4	54·4	1	54·8	1
Al_2O_3	18·5	18·8	18	18·3	18·8	18·4	0·6	18·5	0·6
TiO_2	0·7	0·7	0·7	0·7	0·7	0·7	0·1	0·6	0·1
FeO	7·8	7·3	7·4	8·3	7·4	8·6	0·3	7·9	0·3
MnO	0·2	0·2	0·2	0·2	0·2	0·2	0·1	0·2	0·1
MgO	4·4	4·4	5·3	4·7	3·9	4·4	0·4	3·9	0·4
CaO	4	4·8	4·7	3·5	4	3·6	0·5	3·4	0·5
Na_2O	5·3	4·9	4·8	5·6	5·5	5	0·6	5·8	0·6
K_2O	4·4	4·2	4·3	4·1	4·2	4·8	0·6	4·8	0·6
Total	100	100	100	100	100	100		100	

The melt composition is estimated from XRF analyses of hand-picked groundmass fragments of rocks from the upper and lower chilled zones (XRF), EPMA analyses of fused hand-picked groundmass fragments (EPMA), and mass balance calculation subtracting phenocrysts (Table 5) from the whole-rock composition. The best estimate, representing the average of all the analyses, is given in the first column.

Estimation of conditions in the earliest stage of intrusion

Interstitial melt composition of the chilled zones

The groundmass composition of the chilled margins, which corresponds to the melt composition unmodified by later magmatic differentiation, was estimated by three methods: (1) direct analysis of hand-picked fragments by XRF;(2) EPMA of glass beads obtained by fusion of hand-picked groundmass fragments; (3) mass balance calculations using mineral and whole-rock chemical compositions and phenocryst modes.

The directly measured groundmass compositions of the upper and lower chilled zones are given in Table 7. The uncertainty in the direct analyses is mostly due to the hand-picking procedure. Phenocryst contamination cannot be completely avoided in hand-picking. Method (2) is considered to provide a better composition, because much smaller amounts of fragments are enough for analysis. In method (3), the groundmass composition is estimated by subtracting all phenocrysts (Table 9) from the whole-rock compositions. The calculated interstitial compositions of the upper and lower chilled zones are very similar to those of the direct measurements (Table 7). The similarity is statistically confirmed using the *t*-test (Table 8). It is, therefore, concluded that the initial melt composition of the Nosappumisaki magma was homogeneous at least in the very early stages of emplacement of the sill. This suggests that the difference in phenocryst abundance is responsible for the slight but notable difference in the whole-rock composition of the upper and lower chilled zones. On the basis of the three methods, the best estimation of the melt composition of the intruded magma was obtained by taking their average (Table 7).

Table 8: Result of t*-test to evaluate if the interstitial chemical compositions calculated for the upper and lower chilled zones are the same*

	ν	*t*
wt %		
SiO_2	5	0·48
Al_2O_3	5	0·16
TiO_2	5	0·24
FeO	5	2·42
MnO	5	0·36
MgO	5	1·5
CaO	5	0·49
Na_2O	5	1·65
K_2O	5	0·05

$\alpha = 0{\cdot}02$, $t_\alpha/2(\nu = 21) = 2{\cdot}5$ and $t_\alpha/2(\nu = 40) = 2{\cdot}42$, where t is the t-value, ν is the degree of freedom, and $t_\alpha(\nu)$ is the t-value with degree of freedom ν and adapted confidence coefficient $(1 - \alpha)$.

Table 9: Average chemical compositions of phenocrysts in the chilled zones

	augite	olivine	plagioclase	magnetite
wt %				
SiO_2	50·3	38·0	54·2	—
Al_2O_3	3·97	—	28·30	2·13
TiO_2	0·59	—	0·07	9·56
FeO	7·48	21·71	0·80	79·30
MnO	0·18	—	0·01	2·52
MgO	14·60	39·96	0·07	6·43
CaO	22·30	0·30	11·20	—
Na_2O	0·46	—	4·41	—
K_2O	0·02	—	0·89	—
NiO	0·02	0·07	0·02	—

Some rocks from upper marginal zone I are fine-grained and have no phenocrysts. They occur near the boundary between upper marginal zones I and II. The local phenocryst-free region in upper marginal zone I (Fig. 3d) and the phenocryst-free rocks in the graded layers (Fig. 3b) have identical chemical compositions. The chemical composition of the most fine-grained rock is very similar to that of the groundmass in the chilled zone. These phenocryst-free rocks may have preserved the initial magma composition through complete separation of phenocrysts from the intruded magma, suggesting that there was no spatial chemical variation in the melt, at least within ~10 m from the upper contact during intrusion.

Pressure, temperature, and water content at the time of intrusion

Pressure and temperature conditions and water content in the melt, frozen as the groundmass of the chilled margins, are estimated in this section. Pressure is estimated based on information from the surrounding sedimentary rocks. Some sills occurring along the coast of the Nemuro peninsula are associated with pillow structures (Types 2 and 3), indicating either lava flow onto or intrusion into soft, unconsolidated, sediments (e.g. Yagi, 1969). The Nosappumisaki intrusion and other Type 1 sills, which postdate Types 2 and 3 sills or lava flows, have planar contacts with the host sedimentary rocks and do not show any pillow structures (Fujiwara & Nagase, 1965; Ueda & Aoki, 1968). This is consistent with the inference that these were intruded into host sediments that were almost completely de-watered. On the basis of these observations, the intrusion depth of Type 1 sills is estimated to be 5–7 km, corresponding to the depths at which the porosity of sediments becomes less than a few per cent (Rieke & Chillingarian, 1974; Luo *et al.*, 1993). The sills occur in the lowest horizon of the currently exposed Nemuro formation, which is much greater than 3000 m in thickness. The thickness is consistent with the estimation of the intrusion depth. The pressure of the magma intrusion is, therefore, estimated to be 0·15 ± 0·03 GPa, if the density of sediments is 2600 kg/m^3.

Temperature, water content, and oxygen fugacity of the Nosappumisaki magma are estimated by assuming equilibrium between the phenocryst minerals (Table 9) and the melt, the composition of which is preserved as the groundmass of the chilled margins (Table 7). To constrain the crystallization conditions, olivine–melt and plagioclase–melt equilibrium (including Or content) were examined by calculating equilibrium temperatures for wide ranges of pressure, H_2O content, and oxygen fugacity. In the thermodynamic calculations, solution models for olivine after Hirschmann (1991), for ternary plagioclase after Elkins & Grove (1990), and for silicate melt after Ghiorso & Sack (1995) were adopted. Because the number of independent reactions is greater than the number of variables, a least-squares approach was employed to optimize the conditions. The olivine composition used for the calculation is Fo78·5 from upper marginal zone II (Table 2). A plagioclase composition of An60 Or5, which is observed as clear plagioclase cores in the chilled zones (Table 3), was adopted.

Oxygen fugacity cannot be constrained, but the estimated value based on the FeO and MgO content in plagioclase (Sugawara, 2000) is approximately −9 log units, which corresponds approximately to the nickel–nickel oxide (NNO) buffer at 1125°C. The pressure condition of equilibrium between the olivine and plagioclase phenocrysts and the groundmass melt is constrained to be less than 0·3 GPa, which is consistent with the deeper origin of the 'phenocrysts'. At the possible maximum pressure of 0·3 GPa, the temperature is estimated to be 1125 ± 25°C, and the water content ~1 wt %. If the magma adiabatically ascended to the intrusion site (0·15 GPa), the expected temperature drop is only a few degrees, so that the estimated temperature at the intrusion site was approximately the same as at 0·3 GPa. The water solubility in a melt of the groundmass composition is estimated to be ~3·3 wt % at 0·15 GPa and 1125°C after Moore *et al.* (1998); thus, the magma was undersaturated with water at the time of intrusion. This is consistent with the absence of vesicles in the chilled zones.

By using the estimated pressure, temperature, and water content (0·15 ± 0·03 GPa, 1125 ± 25°C, and 1 wt % of water), the density and viscosity of the intruded melt can be calculated. The density is 2550 ± 100 kg/m^3 according to Lange & Carmichael (1987), and the viscosity (without phenocrysts) is 3·2 ± 0·8 × 10^2 Pas

according to Shaw (1972). The viscosity of the bulk magma including 20 vol. % crystals (chilled margin phenocryst content) is estimated to be $1{\cdot}0 \pm 0{\cdot}5 \times 10^3$ Pas according to the Einstein–Roscoe equation (Shaw, 1965).

Phenocryst abundance in the upper and lower chilled zones

Although the interstitial melt composition was initially homogeneous inside the sill at the start of intrusion, as discussed in the previous section, the phenocryst abundance and its size distribution may not be so, because it is systematically different between the upper and lower chilled zones (Table 5). The difference is mostly attributable to the augite abundance (12 vs 19 vol. %). Augite crystals larger than ~3 mm are absent in the upper chilled zone (Fig. 12), suggesting that phenocryst settling had already begun at the very early stage of intrusion. However, settling was not so extensive in order to keep ~90 vol. % of the initially present phenocrysts in the upper chilled zone. The initial concentration of phenocrysts, which is used in the following discussion, is estimated by simply taking the average of the abundance in the upper and lower chilled zones because one cannot know the exact sorting of phenocrysts (Table 5). The values are similar to the abundances observed in the other intrusions in the Nemuro peninsula and equal the average 'phenocryst' abundance of the whole intrusion, as will be examined below.

Conditions in the later stages of intrusion

Intrusion of the magma took place in a finite time through fracture propagation in the host sedimentary rocks and magma injection. The Nosappumisaki intrusion has no internal chilled margins other than at the roof and floor contacts. Therefore, the intervals of multiple intrusions, if any, were short enough not to form any chilled margins inside the chamber. The observed 'phenocryst' distribution is attributable to redistribution of homogeneously dispersed phenocrysts from a crystal-laden magma frozen as the chilled margins. It might, however, be inappropriate to treat the sill as a closed system characterized by a single homogeneous intrusion, because the melt composition and phenocryst abundance estimated from the chilled margin rocks might not represent the 'initial condition' for the whole magma body. Repeated pulses of new magma with variable melt compositions and phenocryst abundance (Brown, 1956; Irvine & Smith, 1967) or flow differentiation with or without crystal settling (Richardson, 1979) could have occurred. In such cases, the observed crystal distribution in the intrusion reflects either the diversity of the intruding magma or the transportation history during intrusion of the magma but not settling after intrusion (e.g. Gibb & Henderson, 1992).

Table 10: Results of Welch's test to evaluate if the average phenocryst abundance and whole-rock chemical composition in the sill is the same as that of the initial estimation based on the modal abundance in the chilled zones

	Phenocryst modal abundance	
	ν	*t*
augite	38·6	−0·77
olivine	23·8	−0·35
plagioclase	26·1	−1·40
magnetite	21·2	−0·01
phenocryst	30·9	1·45
	Whole-rock composition	
	ν	*t*
SiO_2	38·0	0·04
Al_2O_3	35·1	0·82
TiO_2	38·0	0·07
FeO	33·8	−1·69
MnO	36·0	−1·55
MgO	26·2	−1·58
CaO	29·5	−0·12
Na_2O	27·2	0·40
K_2O	37·9	3·76

$\alpha = 0{\cdot}02$, $t_\alpha/2(\nu = 21) = 2{\cdot}5$ and $t_\alpha/2(\nu = 40) = 2{\cdot}42$, where t is the t-value, ν is the degree of freedom, and $t_\alpha(\nu)$ is the t-value with degree of freedom ν and adapted confidence coefficient $(1 - \alpha)$.

In the following section, it will first be demonstrated that the 'phenocrysts' and melt composition were only internally modified in a closed system, corresponding to the initial conditions estimated in the previous section. Then, the time-scale and frequency of intrusion to attain the total thickness will be examined.

'Phenocryst' abundance and whole-rock composition in the sill

To test if the observed 'phenocrysts' were all derived from a crystal-laden magma with an average phenocryst abundance as estimated above, Welch's test was applied (Table 10, upper section). The test is a statistical analysis for evaluating whether the averages of two statistical populations, with different variances, are equal. Errors

taken into consideration are those in the measurement of modal abundance and in the estimation of the height and local 'phenocryst' concentration. If we adopt a confidence coefficient of 0·98, the average modal abundances in the sill can be regarded as the same as the estimated values from the chilled margins, within the acceptable error range.

It is shown that the average whole-rock chemical composition in the intrusion is indistinguishable from the value of the intruded magma estimated from the chilled zones, by applying Welch's test as in the case for the 'phenocrysts' mass balance (Table 10, lower section). When combined with the mass balance of 'phenocrysts', it is clear that the groundmass composition of the chilled zone is identical to the average composition of the interstitial part of the sill. It is, therefore, concluded that the Nosappumisaki intrusion was derived from a magma with the phenocryst abundance and the melt composition of the chilled zones and that the crystal redistribution process was closed in one dimension.

Intrusion process and 'phenocryst' distribution

A bottom accumulation zone of mafic minerals can be explained by flow differentiation during magma ascent to shallower levels and gravitational crystal settling during lateral transportation (Gibb, 1968, 1972; Komar, 1972*a*, 1972*b*; Marsh, 1988; Mangan *et al.*, 1993; Barker, 2000). During magma ascent in the conduit supplying the sill, crystals are concentrated in the central part and depleted in the marginal parts of the conduit by flow differentiation, forming a crystal-concentrated tongue when the magma is intruded as a sill. The tongue extends laterally above the base of the magma chamber from the entrance site, because of its relatively higher density compared with the crystal-depleted marginal parts (Marsh, 1988; Barker, 2000). If such flow differentiation had occurred in the Nosappumisaki intrusion, a bottom crystal accumulation zone, sharply distinguished from the overlying crystal-free part, should be expected in all the intrusions in the Nemuro peninsula, with the same age and chemical composition as the Nosappumisaki intrusion. The 60 m thick Kinatoishi intrusion, however, lacks a sharp boundary between the accumulation zone and overlying crystal depletion zone (Fig. 14). Moreover, much thinner intrusions (<40 m) have no accumulation zone. The Tosamporo intrusion, which is thinner (80 m) than the Nosappumisaki intrusion, shows no lateral heterogeneity in the thickness of accumulation zone for at least ~500 m. These observations suggest that the accumulation zone in the Nosappumisaki intrusion was not produced by flow differentiation. The presence of a significant amount of phenocrysts in the upper chilled and marginal zones provides further strong evidence against flow differentiation and rapid crystal settling during intrusion.

Crystal settling associated with intrusion is suggested by the difference in modal abundance and size distribution of phenocrysts in the upper and lower chilled margins. This may have continued during intermittent propagation of the sill until its thickness achieved the present thickness. In an extreme case, bottom crystal accumulation could have formed by repeated intrusion pulses of small batches of homogeneous magma with subsequent crystal settling leaving the crystal-free central zone. This intrusion process is expected to produce marked size grading as a result of the development of a crystal-depleted central part, in which collision between crystals and interaction through melt flow become negligible, approaching the ideal Stokes' Law settling behavior. However, size grading is not observed in the cumulate zone, being more consistent with one large intrusion pulse. This is also supported by plagioclase accumulation near the roof, as will be discussed below.

The Kinatoishi intrusion, the thickness of which is half that of the Nosappumisaki intrusion, has an S-shaped 'phenocryst' variation profile (Fig. 14), suggesting that the settling time-scale was comparable with that of solidification (Gray & Crain, 1969; Fujii, 1974). In the case of the intrusions in the Nemuro peninsula, the ratio of the accumulation zone thickness to the total sill thickness increases with the total sill thickness until the sill thickness attains 80 m, but is nearly constant when it is greater than 80 m (Fig. 14c). The thickness of 80 m is inferred to correspond to a limit above which the time-scale of crystal settling is shorter than the cooling time-scale. The systematic relationship suggests that the first intrusion pulse attained at least 80 m in thickness, which corresponds to ~70% of the thickness for the Nosappumisaki intrusion. It is concluded that the intrusion of the Nosappumisaki magma took place as an almost single pulse in a much shorter time than the solidification time-scale.

MECHANISM OF 'PHENOCRYST' REDISTRIBUTION IN THE NOSAPPUMISAKI INTRUSION

In as far as magma emplacement can be regarded as a single event, the 'phenocryst' distribution in the Nosappumisaki intrusion shows that crystal settling was fast enough for most of the crystals to escape capture by the upper solidification front (Marsh, 1988) and that crystal settling did not completely finish before the solidification front reached the 'phenocryst-free' region, which corresponds to the top of the middle zone. The time-scale of solidification of the upper marginal zone and that of crystal settling are, therefore, comparable.

To estimate the time-scale of crystal settling in the crystal-laden Nosappumisaki magma, a simple Stokes' Law settling model is examined first with consideration of additional effects. Then the mechanism of plagioclase concentration in upper marginal zone I is discussed.

Formation of the bottom cumulate pile and overlying crystal-free region

The thickness of the cumulate zone in the intrusions of the Nemuro peninsula (Fig. 1) shows a positive correlation with total sill thickness (Fig. 14b; Takahashi, 1978; Matsui & Yoshimoto, 1987). The composition and phenocryst abundance in the chilled margins of these intrusions are nearly the same and homogeneous, which allows comparison of their 'phenocryst' distributions as a function of sill thickness. The ratio of thickness of the cumulate zone to the total sill thickness is almost constant (Fig. 14c) and approaches ~0·35 when the thickness of intrusion is greater than ~80 m. This ratio is close to that achieved when phenocrysts in a magma with ~20% crystals completely settle forming a bottom accumulation zone with 55% interstitial melt and a phenocryst-free central zone. The ratio decreases as the thickness of the sill decreases from ~80 m, which is the critical thickness to determine whether an intrusion has a clear 'phenocryst-free' region in the central part or not. A thickness of 20–30 m is another critical height, below which a cumulate zone discernible in the field is absent (Fig. 14b; Matsui & Yoshimoto, 1987; Simura, 2004). These observations suggest that competition between crystal settling and inward advancement of the solidification fronts from the roof and bottom boundaries depends on the thickness of the intrusion. From the relation between the total thickness and crystal distribution in the intrusions, the time-scale of formation of the compound structure (combination of the bottom accumulation zone and the overlying crystal-free zone) can be estimated.

Crystal settling or flotation in a sheet-like intrusion of crystal-laden magma is affected by several factors such as density contrast between the crystals and the melt, mechanical mixing driven by forced convection inherited from the intrusion stage, thermal convection driven by heat loss from the top boundary, and the shape and concentration of crystals. The solidification rate is determined by the rate of heat loss through the roof and floor of the sill, which is affected by many factors, such as the thickness of the sill and the vigor of thermal convection. The final crystal distribution in a sill is determined by competition between crystal motion and solidification.

The simplest case for such competition can be examined by combining Stokes' Law with conductive cooling at the upper and lower contacts (Fujii, 1974). The steady-state settling velocity, v_{stokes}, of a spherical particle in an infinite fluid is expressed by the equation

$$v_{stokes} = \frac{2r^2 g(\rho_s - \rho_l)}{9\eta} \quad (1)$$

where v_{stokes} is the Stokes' Law settling velocity, r is the radius of the sphere, ρ_s and ρ_l are the density of crystal and liquid, respectively, g is the gravitational constant, and η is the viscosity of the fluid. The viscosity can be approximated by $\eta = \eta_0 \exp(B_\eta / T)$, where η_0 is the pre-exponential term, T is the temperature in Kelvin, and B_η is a constant (Shaw *et al.*, 1968).

Calculations were carried out first assuming that all the particles were spherical augite phenocrysts with the same diameter and that the temperature of the solidification front was 900°C. The adopted parameters are: thermal diffusivity $\kappa = 5{\cdot}0 \times 10^{-7}$ m^2/s, density difference between crystal and melt $\rho = 700$ kg/m^3, $r = 5{\cdot}0 \times 10^{-3}$ m, $\eta_0 = 10^{-6}$ Pas, and $B_\eta = 2{\cdot}8 \times 10^4$. The calculated vertical variation of particle abundance and its time evolution are shown in Fig. 15. This result indicates that the overall characteristics of the vertical variation of phenocryst abundance depend on the thickness of the sills. Although a certain amount of phenocrysts always settle for any sill thickness (Fig. 15 h), a central region almost free of phenocrysts appears when the sill thickness is greater than ~80 m, as shown in Fig. 15a–e. The calculated thickness of the cumulate pile and the ratio of the thickness of the cumulate pile to the total thickness shown in Fig. 15f and g are comparable with the relationships observed in the studied sills (Fig. 14b and c). For the Nosappumisaki intrusion (120 m in thickness) crystal settling is estimated to have been completed in 10 years in this simplified model, which is the time for grains of average size to completely settle to form an accumulation zone and approximately one-tenth of the total solidification time. Actual particle settling is, however, affected by crystal shape, particle–particle interaction, particle–liquid interaction and convection. These complications are evaluated below.

Several workers have modified equation (1) by considering the effects of particle concentration and shape, interaction among particles, and liquid flow. Richardson & Zaki (1954) experimentally examined the relationship between v_{stokes} and the settling velocity of suspensions v_{susp}, and proposed the equation $v_{susp} = v_{stokes}(1 - \phi)^n$, for cases where particles have the same density and the same size but are concentrated in the fluid, where ϕ is the crystal fraction and n is the exponent parameter ranging from 2·0 to 2·5. In the case of the Nosappumisaki intrusion with 20 vol. % crystals, the Stokes' Law velocity decreases by a factor of 0·56–0·64. The settling velocity of a particle in a dilute fluid decreases as the shape becomes rod-like or disc-like. Kerr & Lister (1991) proposed an equation $v = v_{stokes} S$, where S is a dimensionless

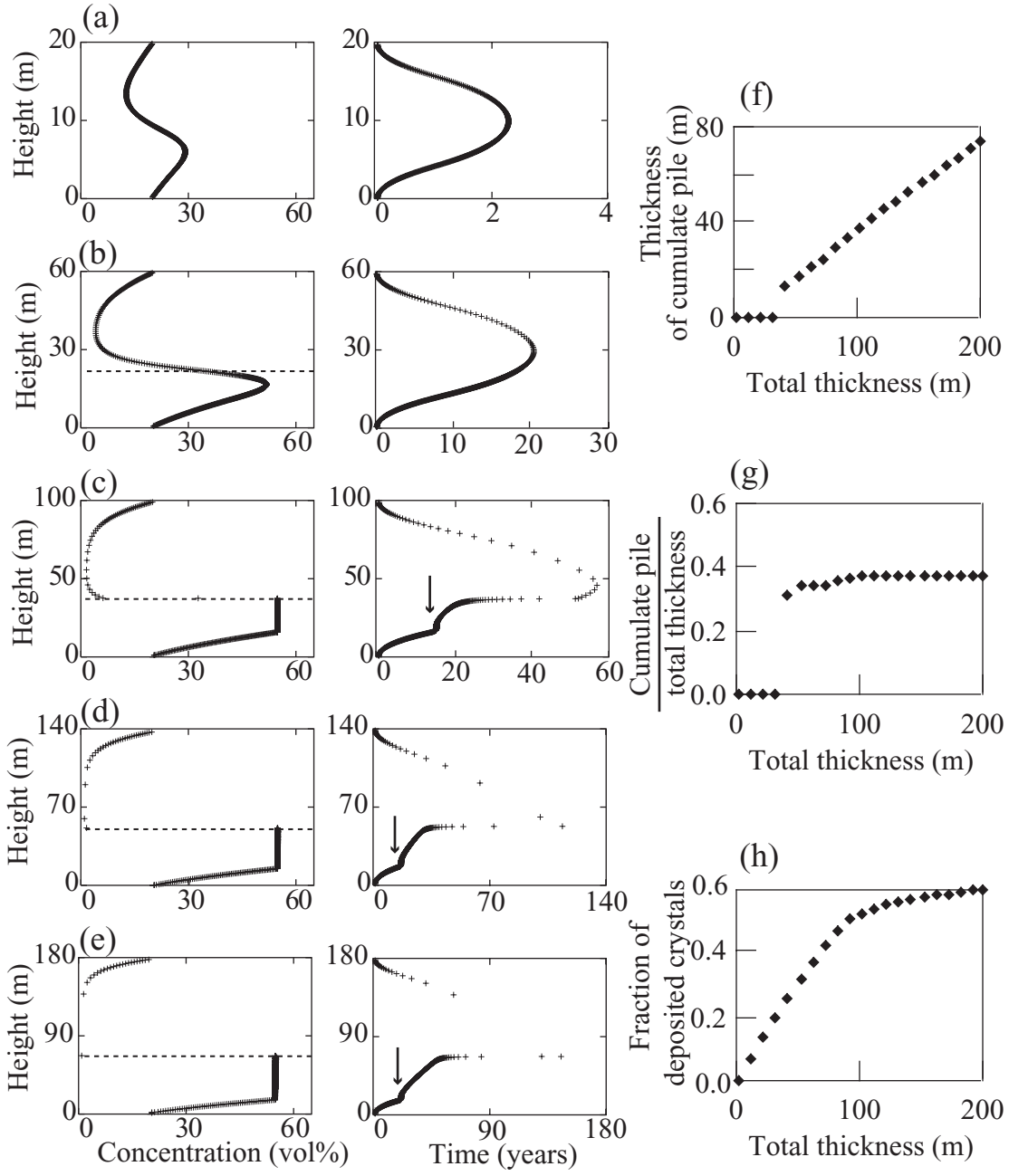

Fig. 15. Modeled crystal distribution during crystal settling in a magma starting from homogeneously distributed, equal-sized crystals (~1 mm) with a concentration of 20 vol. %. Solidification is assumed to proceed from the upper and lower margins by thermal conduction (Fujii, 1974). Frozen vertical variations of phenocryst concentration for various thicknesses [(a) 20 m, (b) 60 m, (c) 100 m, (d) 140 m, (e) 180 m] are shown in the left-hand panels, and the temporal change of the thickness of the upper solidification zone in which the temperature is below the solidification threshold (900°C) and the thickness of the lower solidification zone in the right-hand panels. The latter thickness is defined as the height from the base at which the temperature attains 900°C (temperature-controlled freezing) or the crystal concentration attains 60 vol. % (packaging-controlled freezing). The time when this transition occurs is shown by arrows in (c)–(e), the absence of which in (a) and (b) indicates that freezing is solely due to cooling from below when the thickness is less than 60 m. The thickness of the cumulate pile, the ratio of the cumulate thickness to the total thickness, and the fraction of deposited crystals are plotted against the total thickness in (f), (g), and (h), respectively. The thickness of the cumulate pile plotted in (f) and (g) is defined as the height from the bottom at which the crystal concentration attains 40% (two times the initial concentration) and sharply decreases to a minimum value in the central zone as shown by dashed lines in the frozen profiles of (b) to (e). The thickness can be compared with the observed thickness of the accumulation zone shown by the checkered pattern in Fig. 14.

parameter determining the shape of the crystal and is a function of the axial ratios of an equivalent ellipsoid. The ratio of the three axes of augite in the studied sill is approximately $a:b:c = 1:1:2$, and S is ~0·9 according to Kerr & Lister (1991). Combining this with the concentration effect described above, the settling velocity decreases to nearly half of the Stokes' Law velocity, and the time required to form the bottom accumulation zone and the overlying crystal-free zone in the sill is doubled (17–20 years).

Convection is thought to be another factor affecting particle settling velocity, if the convective velocity is higher than the particle settling velocity predicted in a quiescent condition. Convective velocity depends on crystal concentration in the sill and decreases with increasing crystal concentration, even at concentrations as low as ~1·2 wt %, as shown by the experiments of Koyaguchi *et al.* (1990, 1993). In their experiments, cooled from above, they observed a sharp descending interface between an upper convecting clear region and a lower, non-convecting, crystal-rich region in which there was unimpeded sedimentation, approximately according to Stokes' Law, above a critical initial concentration of particles. The convective disturbance of phenocrysts is thought to be ineffective in crystal-rich regions of the magma. For the Nosappumisaki intrusion with its high initial phenocryst concentration (~20 vol. %; Fig. 11 and Table 5), the effective bulk viscosity is large and thus convection in the suspension during crystal settling is thought to be weak. Therefore, the estimated time-scale, 17–20 years, is more or less plausible for formation of the crystal pile of the Nosappumisaki intrusion on the assumption of negligible acceleration by structural organization of particles, such as coagulation (Schwindinger, 1999) or fluid dynamical instability (Whitmore instability; Whitmore, 1955; Weiland *et al.*, 1984; Batchelor & Janse Van Rensburg, 1986; Marsh, 1988; Druitt, 1995), which will be discussed below.

Absence of size distribution and settling mechanism

Settling of mixtures of particles with a size distribution in a non-dilute fluid suspension was theoretically studied by Greenspan & Ungarish (1982), who claimed that a plane at which crystal size distribution abruptly changes should be developed during settling, which agrees with the experiments of Smith (1966). In their calculation, size grading should be developed in the bottom cumulate pile when the crystals show wide variation in size. In the case of the Nosappumisaki intrusion, however, there is no observation of size grading in the bottom crystal pile (Fig. 12a–d) despite of the wide variation in augite 'phenocryst' size (Fig. 12e–h). This implies that some mechanisms that impede sorting operate during crystal settling in an actual magma containing significant amounts of crystals with a wide size variation.

Particle interactions are inevitable in a concentrated suspension. They are divided into two types: interaction through fluid motion controlled by the distribution or motion of suspended particles and direct interaction such as collision, cluster formation, or coagulation. In the former case of particle interaction through interstitial fluid, it also accelerates or decelerates the settling velocity. Particle motion induces flow of the interstitial melt, and this flow affects the movement of other particles. For example, when two unequal-size spheres settle in a low Reynolds Number fluid, with a large sphere above a small sphere, they settle neither according to Stokes' Law nor following a vertical trajectory, which may hinder crystal sorting. Each sphere settles faster than when it settles alone and follows a curved trajectory as a result of the influence of the other sphere (Han & Lawler, 1991).

In the case of direct interaction, the velocity of particle settling is accelerated or decelerated when particles collide according to the law of conservation of momentum, and the velocity approaches a steady terminal settling velocity according to the density contrast and liquid viscosity. Particle collision could lead to coagulation depending on the surface condition of the particles. When coagulated particles are large and closely packed, the velocity of the coagulated particles is accelerated according to their size, and crystal sorting is significantly suppressed. The opportunity for collision or coagulation increases as the particle concentration increases, but the increase in concentration also limits the space for particle movement. The local concentration of coagulated particles in a limited space results in deposition in intertwined chains of particles, of which the settling velocity is controlled by the chain properties such as connectivity, compactness, and shape. Crystal settling forming these kinds of clusters suppresses crystal sorting as effectively as that forming closely packed coagulations.

When several (more than two) olivine-like prisms settle in an analogue fluid, they tend to form doublets and settle faster than a single prism as shown by Schwindinger (1999). Kaye & Boardman (1962) suggested the formation of larger clusters (triplets, quadruplets, etc.) on the basis of settling experiments using suspensions of small glass spheres in liquid paraffin. In their experiments, the settling velocity increased with an increase of particle concentration up to 3 vol. %, although they observed a decrease in settling velocity at higher particle concentrations as a result of return flow induced by particle settling. Involvement of many particles in this process might lead to settling of loosely packed coagulations or intertwists with various sizes, which may collapse into discrete particles at the bottom.

This settling mechanism could explain the absence of size grading in the bottom cumulate pile of the Nosappumikaski intrusion.

Because convectional velocity is very low near the boundary of the sill, even if strong convection prevails in the central part, phenocrysts will settle according to the velocity predicted in quiescent conditions in such a region (Martin & Nokes, 1989). Therefore, even under strong convection in the central main part, crystals settle near the bottom of the sill under quiescent conditions; thus size grading is inevitable in so far as crystals settle without coagulation or clustering.

As discussed above, coagulation or clustering was probably the most important factor during phenocryst settling in the Nosappumisaki intrusion in suppressing size grading. To evaluate the effects on the crystal size distribution, as well as settling time, a numerical model of crystal settling with coagulation was developed. The basic assumption is that phenocrysts form aggregates at a certain probability when two phenocrysts touch each other. Only vertical motion forming crystal aggregates is considered, to simplify the problem, although lateral segregation of particles with different size and/or density has been considered to be effective in inducing fingering in highly concentrated suspensions of particles with variable density and size (Weiland *et al.*, 1984; see below). Looser aggregation is anticipated in actual cases, but the coagulated particles are assumed to form a new sphere with the combined volume, which increases the radius and consequently the settling velocity. Only a single phase with various size distributions is treated, and, thus, the result is applicable only to the dominant augite 'phenocrysts'.

In the calculation, the dimension of height above the base (h) is scaled by the thickness of the sill, H, and the dimension of time (t) is scaled by the time (t_0) for a particle of average size to settle from the top to the bottom according to Stokes' Law. The position of the ith particle or aggregate is given by the equation

$$h'_i(t') = h'_i(0) - \int_0^{t'} r'_i(t', P)^2 \alpha[\phi(h'_i)]\,\mathrm{d}t' \qquad (2)$$

where $t' = t/t_0$ is the dimensionless time, $h'_i(t') = h_i(t)/H$ is the dimensionless height above the base of a particle at time t, and $r'_i(t', P) = r_i(t, P)/r_{\mathrm{av}}$ is the dimensionless radius of the ith particle normalized to the average particle size, r_{av}. The particle size changes if coagulation occurs according to the sticking probability P. Particle interaction through the fluid is accounted for by the parameter α, which depends on the surrounding particle fraction $\phi(h)$.

It is assumed that crystals are homogeneously distributed in the calculation column with a certain crystal fraction ϕ_0 (= 0·16) at the beginning. The settling velocity of each crystal follows modified Stokes' Law, affected by the surrounding particle fraction. If a crystal is in contact with another crystal, the size and velocity of the new particle is recalculated if they are coagulated. The density and viscosity of the liquid are assumed to be constant in the calculation, and the net motion of fluid as a result of settling is ignored. Although Kaye & Boardman (1962) documented the importance of return flow in particle settling at a high particle concentration, the effect may not be so significant for the most dominant phenocryst (augite) because of its large density contrast with the host melt and the relatively large crystal size. This effect cannot, however, be neglected for plagioclase and will be examined below. It is assumed that crystals are settled if they touch the top of the accumulation zone in which the crystal fraction is 0·55 corresponding to the 'phenocryst' fraction in the cumulate zone. Controlling parameters in the calculation are: sticking probability (P), dimensionless average particle size (r_{av}/H), initial size distribution, initial crystal fraction (ϕ_0), the function for particle interaction through the fluid $\alpha(\phi)$, and the advance rate of the upper solidification front. A Gaussian-like distribution, as well as homogeneous and linearly decreasing initial distributions, was examined. The crystal sizes are separated into 20 discrete divisions.

In Stokes' Law settling, which corresponds to $P = 0$, size grading is distinctively developed in the bottom accumulation zone for any dimensionless average particle size and any particle fraction (Fig. 16a). An obviously size-graded layer is formed, particularly in the upper part of the bottom accumulation zone. The average crystal size at the bottom of the accumulation zone is notably shifted to a larger size than the initial average size (Fig. 16d). Development of a graded layer in the upper part of the accumulation zone is theoretically predicted in simple particle settling in a fluid without consideration of direct particle interaction (e.g. Greenspan & Ungarish, 1982).

If particle coagulation takes place ($P > 0$), size grading in the accumulation zone is suppressed to various degrees according to the sticking probability P. The ratio of the thickness of the graded layer (H_{g}) to the total thickness of the accumulation zone (H_{t}), $H_{\mathrm{g}}/H_{\mathrm{t}}$, decreases with increasing sticking probability (Fig. 16b and c), and the ratio become almost zero when $P > 0{\cdot}2$. For low sticking probability ($P < 0{\cdot}2$ for $\phi_0 = 0{\cdot}16$) the ratio $H_{\mathrm{g}}/H_{\mathrm{t}}$ increases as the initial crystal fraction decreases. When P is greater than zero, particles settle much faster than in Stokes' Law settling (Fig. 16e). The settling time is not affected by P if the sticking probability P is higher than a certain value. The settling time becomes ~1/10 if $P \sim 0{\cdot}2$ for a particle fraction of 0·16.

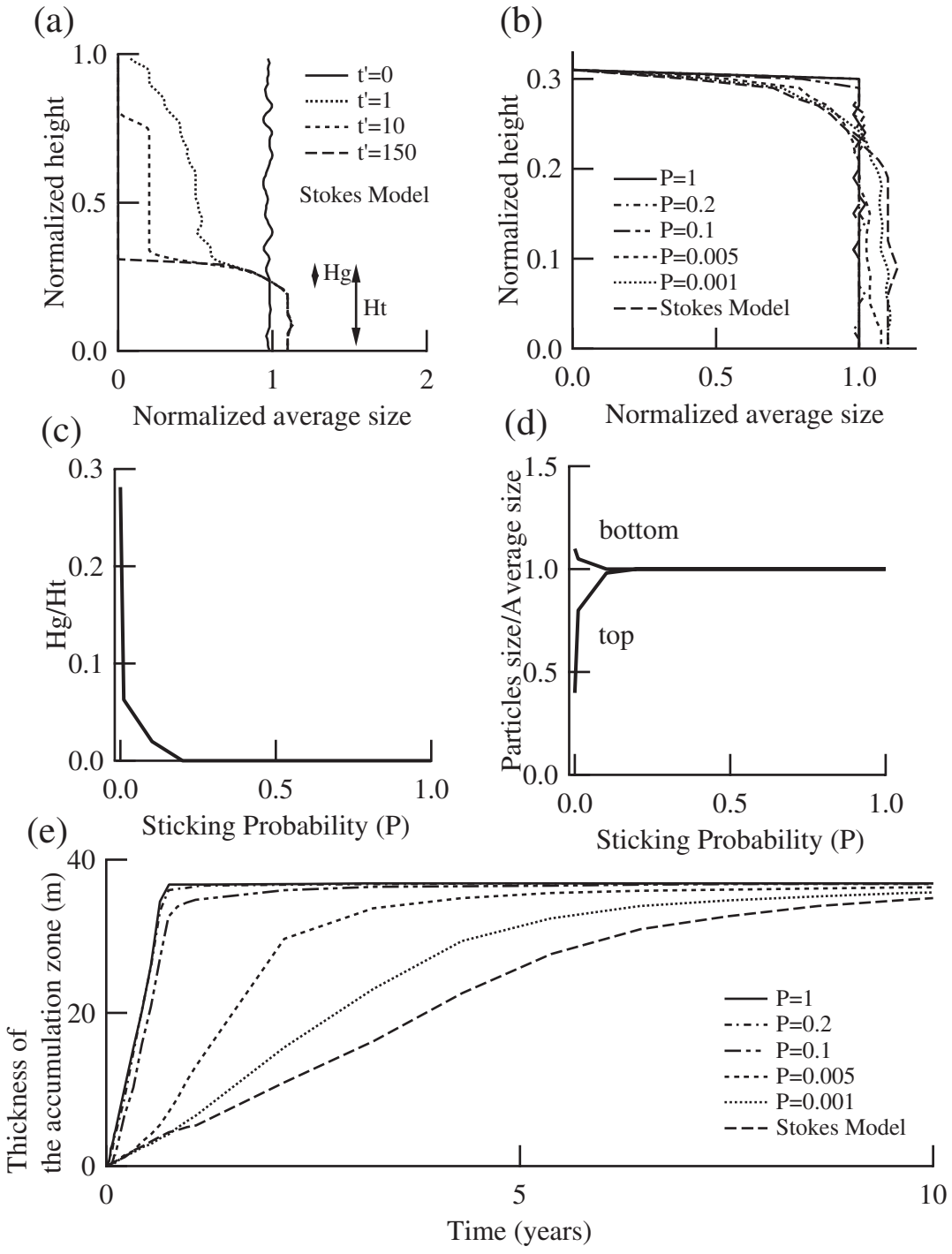

Fig. 16. Modeling results of coagulation settling for a Gaussian-like size distribution and a particle fraction of 0·16. A column height of 120 m and the average particle size of 1 mm are adopted. A temporal change of average particle size for Stokes' Law settling is shown in (a), in which time is normalized to the time for a particle of average size to settle from the top to the bottom according to Stokes' Law. Vertical variations of average particle size after completion of settling are shown in (b) for several values of sticking probability (P). The ratio of the thickness of the graded layer [H_g; see (a)] to the total thickness of the accumulation zone (H_t) is plotted against sticking probability in (c). The normalized average size at the top of the accumulation zone and that at the bottom of the accumulation zone are shown in (d). The temporal increase of the thickness of the bottom accumulation zone is shown in (e), an enlargement of the lower 40 m, for various values of sticking probability.

From the above examination of the particle settling model, it is concluded that a sticking probability greater than 0·2 is required to reproduce the absence of size grading in the cumulate zone of the Nosappumisaki intrusion on the condition that the negligible size grading in the accumulation zone is solely attributed to coagulation during settling. In this case, the settling time-scale must be shorter than that predicted for simple crystal settling according to Stokes' Law (including consideration of particle concentration and particle shape) by a factor of ~1/10 and is a few years. The solidification time-scale of upper marginal zone I must be similar to this estimate because of the entrapment of a smaller amount of augite phenocrysts in this zone. It should be noted that the sticking probability is a model parameter representing all the possible physical processes of settling by coagulating or clustering, and that the value of ~0·2 itself does not have any clear physical significance.

It has been experimentally demonstrated that in concentrated suspensions containing particle species of widely different sizes or densities, each particle species tends to gather together under gravity to develop vertical fingering and finally split-off structures in the bottom accumulation zone and the overlying crystal-free zone (e.g. Whitmore, 1955; Weiland *et al.*, 1984; Batchelor & Janse Van Rensburg, 1986; Marsh, 1988). This kind of fluid dynamical instability increases the settling velocity and could play an important role in actual particle redistribution in crystal-laden magmas. Druitt (1995) examined the instability during settling of non-aggregating, poorly sorted aqueous dispersions and showed that a graded structure is developed unless the initial particle fraction is as high as 50%. Therefore, the instability may not impede size grading for the Nosappumisaki magma even with 20% initial crystals. Although a fluid dynamic instability might have developed in the Nosappumisaki intrusion to accelerate the crystal settling, coagulation or clustering without extensive sorting is necessary to explain the observed absence of grading in the cumulate zone.

Mechanism of plagioclase concentration in the upper part of the sill

Plagioclase is concentrated in upper marginal zone I, where its abundance attains ~10–15 vol. % (Fig. 11). Moreover, the abundance in the upper chilled zone (4 vol. %) is twice as large as that in the lower chilled zone (2 vol. %). The abundance and size of plagioclase in the upper part of the cumulate zone is lower than the average values of the chilled zone (Figs 11 and 12). These observations and the aforementioned conclusion that all the 'phenocrysts', including plagioclase, were redistributed in a one-dimensionally closed system suggest that plagioclase phenocrysts were concentrated in the upper marginal zone by a distinct mechanism. Plagioclase must have been concentrated by flotation, unless it had been already concentrated in the upper part at the time of intrusion, which is an *ad hoc* explanation because plagioclase abundances in the other intrusions are ~8 ± 3·8 vol. % on average in the Nemuro peninsula and because similar plagioclase enrichment near the roof is observed in all these intrusions if their thickness is greater than 60 m. To reproduce the plagioclase abundance in upper marginal zone I from the average modal abundance of the chilled zones (~3 vol. %), plagioclases in the upper 30 m region, almost corresponding to the upper marginal zone, must have been concentrated by flotation. This possibility is examined in this section. First, the density contrast between the melt and plagioclase is considered, and then the mechanism of plagioclase enrichment in the upper part of the sill is discussed using a physical model for concentrated suspensions.

Density difference between plagioclase and the interstitial melt

If the density of plagioclase is smaller than that of the surrrounding melt, the concentration of plagioclase in the upper part of the sill can easily be accounted for. Therefore, it is critical to estimate the density of plagioclase and the melt. The density of plagioclase of composition An59, which is the average value for C-type plagioclase, is around 2650 kg/m^3. This is slightly greater than the density of 2550 × 10 kg/m^3 calculated for the interstitial melt. This density difference predicts that the plagioclase phenocrysts should settle if they behave as a single phase in an infinite medium. This is actually verified by the occurrence of modally graded layering in upper marginal zone II (Figs 2 and 3b). The average total phenocryst abundance is ~6 vol. % in the layering. The upper part of the layer is phenocryst-free and the lower part is relatively rich in plagioclase as well as mafic phases. Some plagioclases (H-type) contain melt inclusions, which decreases their effective density, but such plagioclases are An-rich. For H-type plagioclase with 30 vol. % melt inclusions (the maximum value), the density is estimated to be 2650 kg/m^3, which is the same as that estimated for C-type. The melt density may be less than 2550 kg/m^3 because of the higher concentration of H_2O up to 1 wt %, which decreases the melt density to 2400 kg/m^3 for 2 wt % H_2O. These density estimates negate the possibility of plagioclase flotation if density difference is the only driving force. Plagioclase is definitely denser than any melt that existed in the sills; however, the density contrast is very small (~150 kg/m^3). In contrast, the mafic phenocrysts have much higher density contrasts

(~700–2600 kg/m^3), and these phases do not show noticeable enrichment in the upper part of the sills. This is the key to understanding the mechanism of plagioclase enrichment in upper marginal zone I.

Mechanism of plagioclase enrichment in upper marginal zone I

Plagioclase enrichment in upper marginal zone I took place in the early stage of solidification, when the upper solidification front proceeded downwards to capture the concentrated zone. Otherwise, plagioclase would have completely settled out because of its higher density than the melt.

Because of their large density contrast, the mafic phenocrysts can easily settle out to the floor. However, because plagioclase has a very small density contrast with the melt, it takes much longer to settle out, and thus its transportation may be easily affected by surrounding melt flow. In some situations, lighter or smaller particles can be easily captured by melt flow, such as thermal or compositional convection or flow induced by particle motion (e.g. Martin & Nokes, 1988; Koyaguchi *et al.*, 1990, 1993; Rudman, 1992; Kobaysashi, 1996; Simakin *et al.*, 1997). In the Nosappumisaki intrusion, the phenocryst content is greater than the particle contents described in the above studies; additionally sill-scale convection may not easily occur in magma bodies containing large amounts of phenocrysts because of the marked increase in bulk viscosity. In the next section, another possibility for carrying lighter or smaller particles upward by an upward return flow induced by settling of heavy mafic phenocrysts is examined.

Kynch's sedimentation theory

One-dimensional sedimentation of ideal suspensions of mono-sized spheres under the influence of gravity can be described reasonably well by Kynch's kinematical sedimentation theory (e.g. Kynch, 1952), the principal assumption of which is that the local settling velocity of a particle is a function only of the local volumetric solid concentration. This theory has been expanded for polydisperse suspensions (e.g. Smith, 1965, 1966; Lockett & Al-Habbooby, 1973), the suspension of particles with various densities (e.g. Lockett & Al-Habbooby, 1974), or both (e.g. Masliyah, 1979; Bürger *et al.*, 2000). The equations used in these studies are as follows for each particle species (Wallis, 1969; Masliyah, 1979; Bürger *et al.*, 2000):

$$\frac{\partial \phi_{ij}}{\partial t} + \frac{\partial}{\partial z} f_{ij} = 0 \tag{3}$$

$$f_{ij} = -\phi_{ij}\frac{g}{18\mu_f}V(\phi)\left[d_i^2(\rho_j - \rho_{susp}) - \sum_{h=1}^{N} d_h^2 \sum_{k=1}^{M} \phi_{hk}(\rho_k - \rho_{susp})\right] \tag{4}$$

$$\phi = \sum_{i=1}^{N}\sum_{j=1}^{M}\phi_{ij} \tag{5}$$

$$\rho_{susp} = (1-\phi)\rho_f + \sum_{i=1}^{N}\sum_{j=1}^{M}\phi_{ij}\rho_j \qquad i = 1, 2, \ldots, N;\ j = 1, 2, \ldots, M \tag{6}$$

where ϕ_{ij} and ρ_{ij} are the volumetric concentration and the flux, respectively, of a particle of size d_i and density ρ_j; μ_f is the viscosity of the fluid and z is the vertical coordinate. Subscript susp indicates suspension, and subscript f indicates fluid. $V(\phi)$ is $(1 - \phi)^n$, which is a modified parameter of volumetric flux according to Richardson & Zaki (1954). The velocity of particle transporation, or flux, decreases with increasing local concentration of particles and becomes zero at the critical local concentration of particles.

Equation (6) implies that the local density of the mixture of particles and melt is important as well as the density and size of the particles themselves. The local density of the mixture occasionally becomes higher than that of particles with very low density, if the fluid contains much denser particles. This induces the particle flotation, even if the particle itself is denser than the fluid. This type of flotation was actually observed in the experiments of Richardson & Meikle (1961), but only for high particle concentrations (>8 vol. %). The actual mechanism of flotation of lighter particles is the counter flow induced by the settling of heavier particles (Druitt, 1995). Therefore, flotation is limited to particles that have small density contrast with the melt or particles with very small size and in highly concentrated suspensions.

Application of Kynch's sedimentation theory

The above kind of process is a plausible mechanism to explain plagioclase flotation in the Nosappumisaki intrusion as it has a large amount of heavier phenocrysts. The development of particle distribution in the sill was calculated according to the approach of Bürger *et al.* (2000). In the calculations for the Nosappumisaki intrusion, both the density and concentration of actual 'phenocrysts' were taken into account. The phenocrysts were considered to be homogeneously distributed at the beginning (Fig. 7a). Either mono-sized particles with an

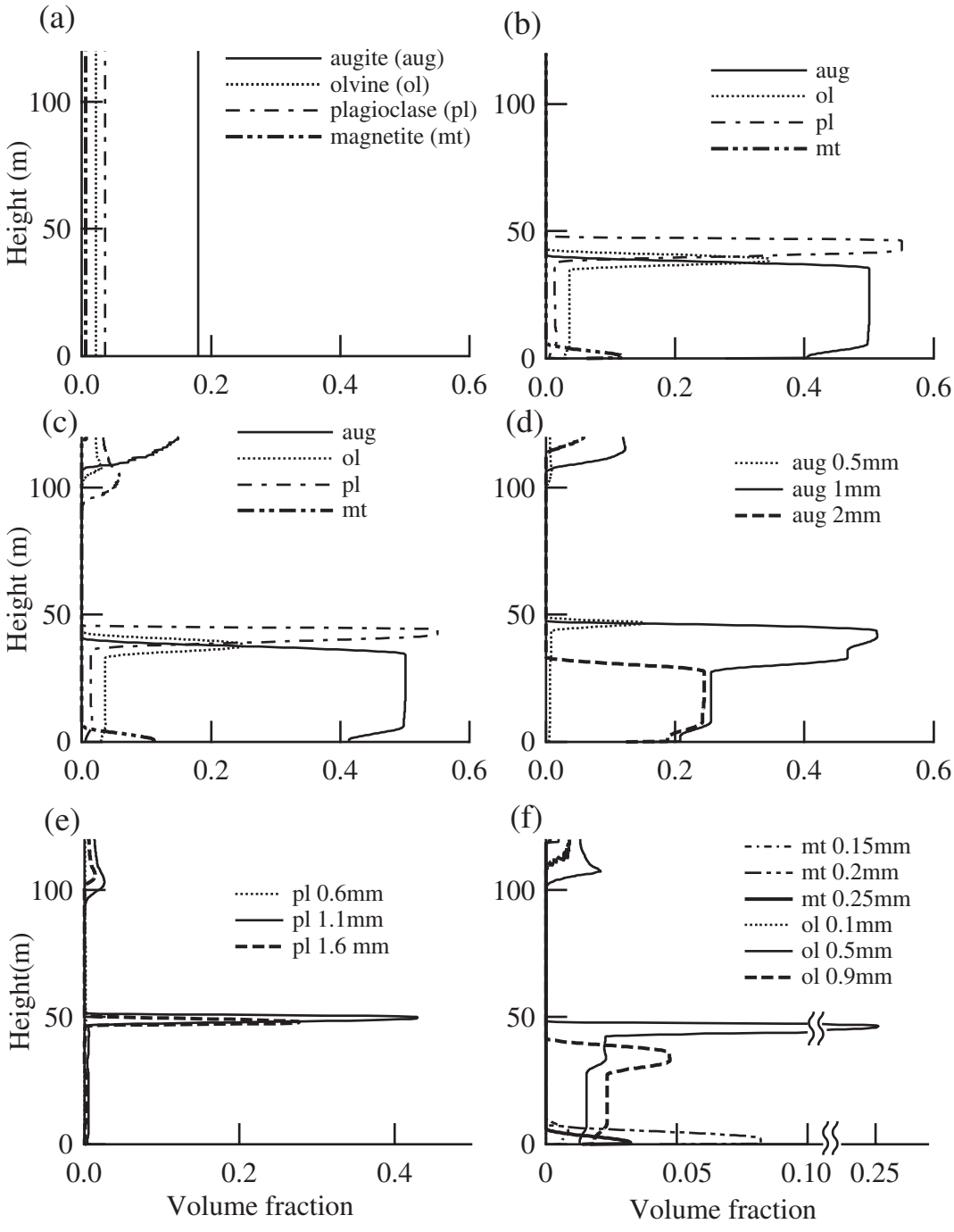

Fig. 17. Results of numerical modeling of redistribution of phenocrysts in a sheet-like intrusion with solidification from both the roof and floor. The adopted model is based on equations (3)–(6) after Bürger *et al.* (2000), which are coupled with equations of thermal conduction to freeze phenocryst motion when temperature attains 900°C. All diagrams except for (a), which shows the initial crystal distribution, illustrate phenocryst distribution after the completion of settling and solidification. Results for mono-sized crystals are shown in (b) and (c); augite = 1 mm, olivine = 0·5 mm, plagioclase = 1·1 mm, and magnetite = 0·2 mm. A reference case without solidification from above is shown in (b). Results for poly-sized crystals are shown in (d) for augite, in (e) for plagioclase, and in (f) for olivine and magnetite. In (d)–(f), three crystal sizes are taken into consideration for each mineral type, in which the size distributions are assumed to be triangular such that the number of grains with an intermediate size is two times that of the largest and smallest sizes. Distributions of the smallest particles cannot be seen in (e) for plagioclase and in (f) for olivine because of their smaller volume fraction. Solidification from the floor is at half the speed of conductive cooling. The density of the liquid is assumed to be 2550 kg/m^3, and the viscosity $3{\cdot}2 \times 10^2$ Pas. The density of plagioclase is 2650 kg/m^3, olivine 3500 kg/m^3, augite 3200 kg/m^3, and magnetite 5200 kg/m^3. The essential features of the calculation results are not significantly affected by the adopted values of the physical properties of melt and minerals.

average size, or several different sizes with a triangular size distribution were assumed for each mineral. The density and viscosity of the interstitial melt are $2550\,kg/m^3$ and $3{\cdot}2 \times 10^2$ Pas. Counter flow from the roof was ignored. Crystal capture by the advancing upper solidification front was also taken into consideration; this is critical because the observed plagioclase concentration cannot be reproduced without capture as a result of cooling from above (Fig. 17b).

The results of the calculation are shown in Fig. 17c–f. The enrichment of plagioclase in the upper horizon can be reproduced by a process of interstitial liquid return flow induced by sinking of heavy particles. In detail, the peak concentration is less than 10 vol. % at most, although the observed value is 10–15 vol. % (Fig. 17c). The maximum concentration of plagioclase cannot exceed the amount of deposited augite phenocrysts because of the volume balance constraint. The augite abundance in the upper chilled zone differs from that in upper marginal zone I by 5–10 vol. % (Fig. 11). Therefore, the higher concentration of plagioclase than that predicted in the model requires other mechanisms. The presence of a very large viscosity contrast near the upper solidification front is one of these mechanisms. A progressive increase in the viscosity towards just beneath the solidification front may cause preferential collection of lighter phenocrysts in the viscous boundary layer. The fairly flattened morphology of plagioclase phenocrysts also affects the efficiency of plagioclase flotation and its capture in the marginal zone. Lateral flow may have caused local concentrations of 'phenocrysts' but is not consistent with the 'phenocryst' mass balance.

Another horizon of high plagioclase concentration appears at the top of the accumulation zone in the model calculation (Fig. 17c and e). Plagioclase grains escape the roof solidification front on top of the accumulation zone, producing a zone with much higher abundance than the original concentration. The high concentration of plagioclase above the crystal pile is actually observed in the Nosappumisaki intrusion (Fig. 11). The observed plagioclase concentration is, however, smaller than expected (compare Fig. 17c and Fig. 11). The calculation results also predict a much smaller amount of plagioclase in the cumulate zone. These inconsistencies are probably attributable to the shapes of the plagioclase phenocrysts, which are far from spherical. Motion in a highly concentrated suspension near the bottom of the settling zone is significantly affected by particle shape. Rectangular parallelepiped-like plagioclase may have difficulty in escaping from the suspension. Coagulation or sweeping by heavier phenocrysts is another possible mechanism to capture plagioclase in the accumulation zone.

The calculation results with a certain initial size distribution show notable size and modal grading in the cumulate zone (Fig. 17d–f), which is not consistent with actual observations (Fig. 11 and Fig. 12e–h). The model considered above is not appropriate to explain the absence of the size grading in the cumulate zone. This is because the direct interaction among particles and the particle shape are not considered. To suppress the size grading in the cumulate zone, direct interaction such as coagulation or clustering is needed during phenocryst settling, as discussed in the previous section.

To produce the high concentration of plagioclase in the upper marginal zone, massive settling of mafic phenocrysts must have taken place, which is more easily attained by one intrusion event in a short time. If multiple intrusions with repeated fracture propagation were involved, upward melt flow might have been weak, because the settling distance is much shorter than the single intrusion event. Even if multiple intrusions were a possible mode of intrusion for the Nosappumisaki intrusion, these must have been relatively few and consecutive so as not to settle most of the plagioclase.

In the one-dimensional modeling expressed by equations (3)–(6), a stable layered structure with a horizontally homogeneous particle distribution is assumed. However, in highly concentrated suspensions containing crystals of widely different sizes or densities, fluid dynamic instability could induce lateral segregation of particle species and vertical streaming or fingering as mentioned above (Whitmore, 1955). Batchelor & Janse Van Rensburg (1986) presented a compilation of experimental results and determined some conditions for such instability in spherical bidisperse systems in terms of four dimensionless parameters: volume fractions of the two types of particles (ϕ_1 and ϕ_2) and the size and density ratios of the two particle species (λ and γ, respectively). By treating all mafic minerals as one particle species and plagioclase as another species, these four parameters are found to be $\phi_1 \sim 0{\cdot}033$, $\phi_2 \sim 0{\cdot}18$, $\lambda \sim 1{\cdot}0$, and $\gamma \sim 0{\cdot}15$ for the Nosappumisaki intrusion. As this parameter combination is not in the parameter space compiled by Batchelor & Janse Van Rensburg (1986), it is uncertain whether or not instability occurred in the Nosappumisaki magma. If such instability actually took place, it is expected that plagioclase crystals would be more efficiently separated from the sinking zone of mafic minerals and more quickly transported towards the roof. Vertical streaming might have caused higher concentration of plagioclase phenocrysts in the upper marginal zones than expected from the one-dimensional model based on Kynch's kinematic theory; this is more consistent with the observations. The non-spherical morphology of 'phenocrysts', particularly platy plagioclase, is another factor that enhances the instability, as experimentally shown in the clumping of fiber suspensions (Herzhaft *et al.*, 1996; Mackaplow & Shaqfeh, 1998).

DISCUSSION

Pre-existing 'phenocrysts' accumulation

In the Nosappumisaki intrusion, plagioclase 'phenocrysts' are concentrated in the upper horizon, which is most plausibly explained by flotation of plagioclase as a result of upward currents induced by massive settling of heavier mafic phenocrysts. Floated plagioclase phenocrysts were captured by the downward propaging upper solidification front. This phenomenon may occur in a deep magma body where the plagioclase density is higher than, but very close to, the melt density. In this discussion, the possibility of plagioclase flotation is generalized and the criterion to determine if plagioclase can float or sink is presented.

Plagioclase flotation and sedimentation have long been discussed because plagioclase accumulation is sometimes observed in both the lower and upper parts of layered intrusions (e.g. Campbell, 1978; Irvine, 1987; Huppert & Sparks, 1984). Kushiro & Fujii (1977) experimentally showed the possibility of plagioclase flotation at high pressure and concluded that massif-type anorthosite intrusions formed at relatively deeper levels in the continental crust. Their arguments, however, focused only on the density contrast between plagioclase and silicate melt, which is controlled by the chemical composition of the plagioclase and the silicate melt as well as pressure and temperature. The above discussions may, however, be oversimplifications, because plagioclase can float even if its density is greater than that of the melt as discussed above.

Let us consider a situation where plagioclase floats driven by the return flow caused by settling of heavier crystals. The plagioclase velocity depends on the abundance ratio of light crystals to heavier crystals. Crystal transportation may obey the settling equations described by Bürger *et al.* (2000), if particle interactions can be ignored. The crystal concentration of plagioclase should satisfy the equations

$$\rho_{pl} - \rho_{susp} < 0 \tag{7}$$

$$\rho_{susp} = \rho_{liq}\phi_{liq} + \rho_{pl}\phi_{pl} + \sum_{min}\rho_{min}\phi_{min} \tag{8}$$

where ρ_i is the density and subscript pl stands for plagioclase, susp for suspension, liq for liquid, and min for minerals other than plagioclase. Equation (7) becomes as follows by substituting equation (8):

$$\sum_{min}\Delta\rho_{min}\phi_{min} > \Delta\rho_{pl}(1-\phi_{pl}) \tag{9}$$

where $\Delta\rho_i$ is the density contrast between the liquid and the ith mineral, $\rho_i - \rho_{liq}$. It is plausible that this condition is satisfied for plagioclase because its density is always close to that of the coexisting silicate melt.

Let us assume a basaltic magma of density 2600 kg/m^3 containing olivine of density 3500 kg/m^3 and plagioclase of 2700 kg/m^3; plagioclase crystals float when the total concentration of olivine exceeds ~10 vol. %. The effect considered here should become noticeable for the Nosappumisaki intrusion which initially contained 16 vol. % augite and 2·4 vol. % olivine. The 10–20 vol. % of mafic phenocrysts is common for basaltic magmas, thus the effect of highly concentrated suspensions should be considered to decide if plagioclase floated or settled in a magma body.

It should also be noted that, to keep plagioclase at a high level in an intrusion, the floated plagioclase must be captured in the upper solidification front. Otherwise, plagioclase would settle following the settling of the mafic phases. Another point to note is that this phenomenon occurs when a mixture of plagioclase and mafic minerals is supplied into a magma chamber in a very short time. This mechanism promotes plagioclase–mafic mineral separation to form modal grading that is much sharper than would be expected only from the density contrast.

Coagulation and size grading in the intrusions

According to the numerical experiments, the crystal pile of thickness H_t in the bottom of an intrusion, which is formed by crystal settling, is divided into two regions: the upper size-graded layer of thickness H_g and the lower layer with homogeneous crystal size and thickness $H_h = H_t - H_g$. The position or the ratio of the interface between the two regions (H_g/H_t) does not depend on the total height of the sedimentation column, which is the actual thickness of the intrusion, but depends only on the initial particle size distribution and the initial particle fraction when the sticking probability is zero (Greenspan & Ungarish, 1982). Let us assume an intrusion of 100 m thickness, an initial particle fraction of 0·1, and the same single crystal size and viscosity of magma as in the intrusions of the Numero peninsula. The thickness of the upper size-graded layer becomes 10 m when coagulation does not occur without solidification from above. Size grading in the layer must be obvious, and the average crystal size in the bottom of the layer is four times larger than that in the top of the layer. On the other hand, when the sticking probability of coagulation exceeds a certain value (0·2 in this calculation) the thickness of the upper graded part is less than 2 m. Size grading in the layer is not obvious and the average crystal size in the bottom is less than 1·3 times larger than that in the top. The thickness and size grading

become ambiguous when solidification from the roof is considered.

Many small igneous intrusions with S-shaped vertical variations in modal abundance (Mangan & Marsh, 1992) have no clear or recognizable size grading in the bottom cumulate pile (e.g Hurlbut, 1937; Wilshire, 1967; Moore & Evans, 1967; Fujii, 1974). To explain the absence of size grading, the sticking probability during phenocryst settling in such intrusions should be greater than a certain value (0·2 in this calculation), if pre-existing phenocrysts were homogeneously distributed before crystal settling commenced.

Crystal settling and compaction

In the initial stage of crystal settling in a concentrated suspension, individual crystals can move freely. When the particle concentration exceeds a critical value, crystals interconnect to form a network, in which the motion of each crystal is strongly confined but subsidence as a whole is still possible through compaction driven by gravitational or tectonic forces. The compaction advances by modification of the framework structure until the rate of subsidence significantly decreases to form a rigid framework, in which the particle concentration ranges from 25 to 60%, according to the particle shape and the thickness of the crystal pile. Philpotts *et al.* (1998) experimentally showed that plagioclase can form frameworks even at a modal abundance of 25 vol. % because of its platy shape. This rigid but loose framework was actually formed in sills and lava flows in the Hartford basin, where compaction is believed to have been the major mechanism of magmatic fractionation (Philpotts *et al.*, 1996, 1998; Boudreau & Philpotts, 2002).

If the magmas forming the Nosappumisaki and other intrusions in the Nemuro peninsula were loaded with ~20% plagioclase with minor mafic minerals, then crystal redistribution might have been governed by compaction after forming a framework of platy plagioclase by short-term crystal settling. This process might have suppressed size grading in the cumulate zone. However, in the studied sills, the dominant phenocryst is augite with a rounded shape. Such a crystal shape requires higher crystal fractions to form 'very loose random packing', which is attained when the fluid velocity is slowly reduced in a fluidized bed: ~44 vol. % for a mono-sized sphere (Haughey & Beveridge, 1969). It is concluded, therefore, that crystal settling in a concentrated suspension was the major process in the studied intrusions. Compaction could have taken place, but only after the completion of crystal settling to attain a 'phenocryst' fraction very close to the current value of 50 vol. % for the cumulate zone. The enrichment of plagioclase phenocrysts near the roof in the studied sills also supports this conclusion. Pipe-like structures observed in the cumulate zone are inferred to have formed after crystal settling was almost completed, possibly accompanied by compaction of the resultant crystal mush.

Graded layering and instability in a crystal-laden magma

Phenocryst-free horizons, locally developed in the upper marginal zones of the Nosappumisaki intrusion (Fig. 3d), may represent melt pools from which phenocrysts were completely eliminated by a certain type of instability. Graded layering observed in the same zone (Fig. 3b) is inferred to be a structure in which the continuing process of amplification of this instability was frozen. This is supported by the presence of ~1 m thick reverse grading on top of a set of normally graded layers of 10–40 cm thickness, suggesting subsidence of the layered portion relative to the host, which has a homogeneous distribution of phenocrysts. The graded layering is inferred to represent a kind of kinematic shock, which is expected to develop during settling of a non-dilute fluid suspension containing particles with different densities and/or sizes (Greenspan & Ungarish, 1982; Marsh, 1988).

In a particle-concentrated suspension, fluid dynamical instability could induce a particle-laden current, which is one of the most effective mechanisms to redistribute crystals in magma bodies (e.g. Marsh, 1998; Druitt, 1995). This process probably operated during the main stage of crystal redistribution to enhance the plagioclase enrichment in upper marginal zone I as discussed above, but is not responsible for the formation of the observed phenocryst-free portions in the upper marginal zones because of the absence of evidence for horizontal segregation and upward streaming compensating descending phenocryst-laden currents. It is inferred that phenocrysts in the upper marginal zones escaped capture of the upper solidification front with 5–10 vol. % phenocrysts in the final stage of solidification only via particle-concentrated currents induced by multiphase Rayleigh–Taylor instabilities (Bergantz & Ni, 1999; Michioka & Sumita, 2005).

SUMMARY

Crystals in the Nosappumisaki intrusion can be divided into two types: 'phenocrysts' already present at the time of intrusion and crystals formed *in situ* after intrusion. Such clear discrimination is not usually possible, and this advantage of the Nosappumisaki intrusion provides a testable case of crystal settling/flotation in a real magma chamber. The observed textural features of the 'phenocrysts' in the accumulation zones indicate that overgrowth was fairly limited before they were captured

by the roof solidification front or accumulated on the floor, allowing us to regard 'phenocrysts' as non-reactive particles during their transportation. Critical observations regarding crystal redistribution in the intrusion are the absence of size grading in the accumulation zone and the high concentration of plagioclase near the upper contact.

The initial temperature and pressure conditions at the time of intrusion of the Nosappumisaki intrusion are estimated to be 1125 ± 25°C and 0·15 ± 0·03 GPa. The magma had ~1 wt % H_2O with a phenocryst abundance of ~20 vol. %. The spatial homogeneity of the intruded magma in terms of chemical composition and phenocryst abundance is confirmed from several lines of evidence from the Nosappumisaki intrusion and other sills in the Nemuro peninsula. This allows us to model crystal redistribution in one dimension starting from a homogeneous spatial distribution. Coagulational settling of phenocrysts is required to explain the absence of grading in the bottom cumulate pile in the Nosappumisaki intrusion. The coagulation or clustering also shortens the duration of deposition, leading to massive settling in a few years if the most compact coagulation is assumed. The time-scale is approximately equal to the solidification time of the upper marginal zones. Furthermore, massive phenocryst deposition generated a counter flow, and this caused flotation of plagioclase, despite its slightly higher density than the interstitial melt. This process produced high concentrations of plagioclase phenocrysts in the upper marginal zone of the Nosappumisaki and other shoshonite sills in the Nemuro peninsula. Crystal transportation in a magma body is strongly affected by crystal–crystal direct interaction and crystal-flow interaction caused by the crystal transportation itself.

ACKNOWLEDGEMENTS

We thank H. Nagahara, H. Iwamori, T. Koyaguchi, T. Fujii, and T. Kuritani for fruitful discussions. Comments from three reviewers—R. C. Kerr, O. Backmann, and R. A. Wieve—were very helpful in improving the manuscript. We thank R. C. Kerr for drawing our attention to the fluid dynamic instability in particle settling of highly concentrated suspensions. Editorial handling by D. Geist is greatly appreciated. R.S. is grateful to Hideto Yoshida for EPMA and XRF analyses. R.S. also thanks the people of Nemuro City, especially those of the Nemuro Fishery Laboratory, for providing housing in Nemuro, and those of the Preparative Office of the Nemuro Municipal Museum for providing access to some documents. This work was supported by the Japanese Society for the Promotion of Science for Japan Junior Scientists.

REFERENCES

Barker, D. S. (2000). Emplacement of a xenolith-rich sill, Lajitas, Texas. *Journal of Volcanology and Geothermal Research* **104**, 153–168.

Barnea, E. & Mizrahi, J. (1973). A generalized approach to the fluid dynamics of particulate systems. Part I. General correlation for fluidization and sedimentation in solid multiparticle systems. *Chemical Engineering Journal* **5**, 171–189.

Batchelor, G. K. (1982). Sedimentation in a dilute polydisperse system of interacting spheres. Part 1. General theory. *Journal of Fluid Mechanics* **119**, 379–408.

Batchelor, G. K. & Janse Van Rensburg, R. W. (1986). Structure formation in bidisperse sedimentation. *Journal of Fluid Mechanics* **166**, 379–407.

Bence, A. E. & Albee, A. L. (1968). Empirical correction factors for the electron micro-analysis of silicates and oxides. *Journal of Geology* **76**, 382–403.

Bergantz, G. W. & Ni, J. (1999). A numerical study of sedimentation by dripping instabilities in viscous fluids. *International Journal of Multiphase Flow* **25**, 307–320.

Boudreau, A. & Philpotts, A. R. (2002). Quantitative modeling of compaction in the Holyoke flood basalt, Hartford Basin, Connecticut. *Contributions to Mineralogy and Petrology* **144**, 176–184.

Bowen, N. L. (1928). *Evolution of the Igneous Rocks*. Princeton, NJ: Princeton University Press.

Brandeis, G. & Marsh, B. D. (1989). The convective liquidus in a solidifying magma chamber—a fluid dynamic investigation. *Nature* **339**, 613–616.

Brown, G. M. (1956). The layered ultrabasic rocks of Rhum, Inner Hebrides. *Philosophical Transactions of the Royal Society of London, Series B* **240**, 1–53.

Bürger, R., Concha, F., Fjelde, K. K. & Karlsen, K. H. (2000). Numerical simulation of the settling of polydisperse suspensions of spheres. *Powder Technology* **113**, 30–54.

Campbell, I. H. (1978). Some problems with the cumulus theory. *Lithos* **11**, 311–323.

Carman, M. F. (1994). Mechanisms of differentiation in shallow mafic alkaline intrusions, as illustrated in the Big Bend area, western Texas. *Journal of Volcanology and Geothermal Research* **61**, 1–44.

Carman, M. F., Dietrich, V. J. and Sommerauer, J. (1984). Petrography and mineral chemistry of basalts from Holes 519A, 520, 522B, and 524—Leg 73 (South Atlantic) of the Deep Sea Drilling Project. Initial Reports of the Deep Sea Drilling Project 73, 545–577.

Caroff, M., Ambrics, C., Maury, R. C. & Cotten, J. (1997). From alkali basalt to phonolite in hand-size samples: vapor-differentiation effects in the Bouzentes lava flow (Canta, France). *Journal of Volcanology and Geothermal Research* **79**, 47–61.

Davis, R. H. & Acrivos, A. (1985). Sedimentation of noncolloidal particles at low Reynolds numbers. *Annual Review of Fluid Mechanics* **17**, 91–118.

Davis, R. & Gecol, R. (1994). Hindered settling function with no empirical parameters for polydisperse suspensions. *AIChE Journal* **40**, 570–575.

Doheim, M. A., Abu-Ali, M. H. & Mabrouk, S. A. (1997). Investigation and modelling of sedimentation of mixed particles. *Powder Technology* **91**, 43–47.

Druitt, T. H. (1995). Settling behaviour of concentrated dispersions and some volcanological applications. *Journal of Volcanology and Geothermal Research* **65**, 27–39.

Elkins, L. T. & Grove, T. L. (1990). Ternary feldspar experiments and thermodynamic models. *American Mineralogist* **75**, 544–559.

Fujii, T. (1974). Crystal settling in a sill. *Lithos* **7**, 133–137.

Fujiwara, T. & Mitani, K. (1959). *The geological map of 1:50 000, Nosappumisaki region*. Geological Survey Institute of Hokkaido Government, Sappro, Japan.

Fujiwara, Y. & Nagase, M. (1965). Paleomagnetic studies on the Cretaceous rocks in the Nemuro Peninsula, Hokkaido, Japan. *Earth Science (Chikyu Kagaku)* **79**, 42–46.

Ghiorso, M. S. & Sack, R. O. (1995). Chemical mass-transfer in magmatic processes IV. A revised and internally consistent thermodynamic model for the interpolation and extrapolation of liquid–solid equilibria in magmatic systems at elevated temperatures and pressures. *Contributions to Mineralogy and Petrology* **119**, 197–212.

Gibb, F. (1968). Flow differentiation in the xenolithic ultrabasic dikes of the Cuillins and the Strathaird Peninsula, Isle of Skye, Scotland. *Journal of Petrology* **9**, 411–443.

Gibb, F. (1972). A differentiated ultrabasic sheet on Sgurr Dearg, Isle of Skye. *Mineralogical Magazine* **38**, 811–818.

Gibb, F. G. F. & Henderson, C. M. B. (1992). Convection and crystal settling in sills. *Contributions to Mineralogy and Petrology* **109**, 538–545.

Goff, F. (1996). Vesicle cylinders in vapor-differentiated basalt flows. *Journal of Volcanology and Geothermal Research* **71**, 167–185.

Goto, Y. (1996). A rhythmically banded basaltic andesite intrusion in the Shiretoko Peninsula, Hokkaido, Japan. *Journal of Mineralogy, Petrology and Economic Geology* **91**, 427–442.

Gray, N. & Crain, I. (1969). Crystal settling in sills; a model for suspension settling. *Canadian Journal of Earth Sciences* **6**, 1211–1216.

Greenspan, H. & Ungarish, M. (1982). On hindered settling of particles of different sizes. *International Journal of Multiphase Flow* **8**, 587–604.

Han, M. & Lawler, D. (1991). Interactions of 2 settling spheres—settling rates and collision efficiency. *Journal of Hydraulic Engineering—ASCE* **117**, 1269–1289.

Hartman, M., Trnka, O. & Svoboda, K. (1994). Free settling of non spherical particles. *Industrial and Engineering Chemistry Research* **33**, 1979–1983.

Haughey, D. P. & Beveridge, G. S. G. (1969). Structural properties of packed beds—a review. *Canadian Journal of Chemical Engineering* **47**, 130.

Herzhaft, B., Guazzelli, E., Mackaplow, M. B. & Shaqfeh, S. G. (1996). Experimental investigation of the sedimentation of a dilute fiber suspension. *Physical Review Letters* **77**, 290–293.

Hirschmann, M. (1991). Thermodynamics of multicomponent olivines and the solution properties of $(Ni,Mg,Fe)_2SiO_4$ and $(Ca,Mg,Fe)_2SiO_4$ olivines. *American Mineralogist* **76**, 1232–1248.

Huppert, H. & Sparks, S. (1984). Double-diffusive convection due to crystallization in magmas. *Annual Review of Earth and Planetary Sciences* **12**, 11–37.

Huppert, H. E. & Sparks, R. S. J. (1989). Chilled margins in igneous rocks. *Earth and Planetary Science Letters* **92**, 397–405.

Hurlbut, C. S. (1937). Igneous rocks of the Highwood Mountains, Montana. *Geological Society of America Bulletin* **50**, 1043–1112.

Irvine, T. & Smith, C. (1967). The ultramafic rocks of the Muskox intrusion, Northwest Territories, Canada. In: Wyllie, P. J. (ed.) *Ultramafic and Related Rocks*. New York: John Wiley, pp. 38–49.

Irvine, T. N. (1987). Layering and related structures in the Duke Island and Skaergaard intrusions: similarities, differences and origins. In: Parsons, I. (ed.) *Origins of Igneous Layering*. Dordrecht: D. Reidel, pp. 185–245.

Jaupart, C. & Brandeis, G. (1986). The stagnant bottom layer of convecting magma chambers. *Earth and Planetary Science Letters* **80**, 183–199.

Jaupart, C., Brandeis, G. & Allègre, C. J. (1984). Stagnant layers at the bottom of convecting magma chambers. *Nature* **308**, 535–538.

Jeffrey, D. & Onishi, Y. (1984). Calculation of the resistance and mobility functions for two unequal rigid spheres in low-Reynolds-number flow. *Journal of Fluid Mechanics* **139**, 261–290.

Jeyaweera, K. O. L. F. & Mason, B. J. (1965). The behaviour of freely falling cylinder and cones in a viscous fluid. *Journal of Fluid Mechanics* **22**, 709–720.

Kaye, B. & Boardman, R. (1962). Cluster formation in dilute suspensions. In: Rottenburg, P. A. (ed.) *Symposium on the Interaction between Fluids and Particles*. London: Institution of Chemical Engineers, pp. 17–21.

Kerr, R. C. & Lister, J. R. (1991). The effects of shape on crystal settling and on the rheology of magmas. *Journal of Geology* **99**, 457–467.

Kerr, R. C., Woods, A. W., Worster, M. G. & Huppert, H. E. (1989). Disequilibrium and macrosegregation during solidification of a binary melt. *Nature* **340**, 357–362.

Kiminami, K. (1978). Reconsideration of the stratigraphy of the Nemuro formation. *Earth Science (Chikyu Kagaku)* **32**, 120–132.

Kiminami, K. (1983). Sedimentary history of the late Cretaceous–Paleocene Nemuro Group, Hokkaido, Japan: a forearc basin of the Paleo-Kuril arc–trench system. *Journal of the Geological Society of Japan* **89**, 607–624.

Kimura, G. & Tamaki, K. (1986). Collision, rotation, and back-arc spreading in the region of the Okhotsk and Japan seas. *Tectonics* **5**, 389–401.

Kirkpatrick, R. J., Robinson, G. R. & Hays, J. F. (1976). Kinetics of crystal growth from silicate melts: anorthite and diopside. *Journal of Geophysical Research* **81**, 5715–5720.

Kobaysashi, S. (1996). Fluid motion induced by flotation/sedimentation of immiscible particles—applications to magmatic convection. *Memoirs of the Geological Society of Japan* **46**, 43–57.

Komar, P. D. (1972*a*). Mechanical interactions of phenocrysts and flow differentiation of igneous dikes and sills. *Geological Society of America Bulletin* **83**, 973–988.

Komar, P. D. (1972*b*). Flow differentiation in igneous dikes and sills: profiles of velocity and phenocryst concentration. *Geological Society of America Bulletin* **83**, 3443–3448.

Koyaguchi, T., Hallworth, M., Huppert, H. & Sparks, R. (1990). Sedimentation of particles from a convecting fluid. *Nature* **343**, 447–450.

Koyaguchi, T., Hallworth, M. A. & Huppert, H. (1993). An experimental study on the effects on phenocrysts on convection in magmas. *Journal of Volcanology and Geothermal Research* **55**, 15–32.

Kushiro, I. (1994). Analysis of major and minor elements in silicate rocks with X-ray fluorescence. In: *Evolution of the Crust in Island Arcs*. Grant Report for the Ministry of Education of Japan, pp. 1–22.

Kushiro, I. & Fujii, T. (1977). Flotation of plagioclase in magma at high pressures and its bearing on the origin of anorthosite. *Proceedings of the Japan Academy* **53**, 262–266.

Kynch, G. J. (1952). A theory of sedimentation. *Transactions of the Faraday Society* **48**, 166–176.

Kynch, G. J. (1958). The slow motion of two or more spheres through a viscous fluid. *Fluid Mechanics* **5**, 193–208.

Lange, R. A. & Carmichael, I. (1987). Densities of Na_2O–K_2O–CaO–MgO–FeO–Fe_2O_3–Al_2O_3–TiO_2–SiO_2 liquids: new measurements and derived partial molar properties. *Geochimica et Cosmochimica Acta* **51**, 2931–2946.

Lindsley, D. H. (1983). Pyroxene thermometry. *American Mineralogist* **68**, 477–493.

Lockett, M. & Al-Habbooby, H. (1973). Differential settling by size of two particle species in a liquid. *Transactions of the Institution of Chemical Engineerings* **51**, 281–292.

Lockett, M. & Al-Habbooby, H. (1974). Relative particle velocities in two-species settling. *Powder Technology* **10**, 67–71.

Luo, X., Brigud, F. & Vasseur, G. (1993). Compaction coefficients of argillaceous sediments: their implications, significance and determination. In: Doré, A. G., Augustson, J.H., Hermanrud, C., Stewart, D.J. & Sylta, O. (eds) *Basin Modelling: Advances and Applications*. Amsterdam: Elsevier, pp. 321–332.

Mackaplow, M. B. & Shaqfeh, E. S. G. (1998). A numerical study of the sedimentation of fibre suspensions. *Journal of Fluid Mechanics* **376**, 149–182.

Mangan, M. & Marsh, B. (1992). Solidification front fractionation in phenocryst-free sheet-like magma bodies. *Journal of Geology* **100**, 605–620.

Mangan, M., Marsh, B., Froelich, A. & Gottfried, D. (1993). Emplacement and differentiation of the York Haven diabase sheet, Pennsylvania. *Journal of Petrology* **34**, 1271–1392.

Marsh, B. D. (1988). Crystal capture, sorting, and retention in convecting magma. *Geological Society of America Bulletin* **100**, 1720–1737.

Marsh, B. D. (1996). Solidification fronts and magmatic evolution. *Mineralogical Magazine* **60**, 5–40.

Martin, D. & Nokes, R. (1988). Crystal settling in a vigorously convecting magma chamber. *Nature* **332**, 534–536.

Martin, D. & Nokes, R. (1989). A fluid dynamic study of crystal settling in convecting magmas. *Journal of Petrology* **30**, 1471–1500.

Masliyah, J. (1979). Hindered settling in a multiple-species particle system. *Chemical Engineering Science* **34**, 1166–1168.

Matsui, N. & Yoshimoto, Y. (1987). Geology and petrology in Nemuro City. In: *Nature and Cultural Assets in Nemuro City*. Nemuro City, Japan: Committee of Education in Nemuro City 1–37.

Matsumoto, T. (1970). Geological age of Mesozoic. *Earth Science (Chikyu Kagaku)* **40**, 248–255.

Michioka, H. & Sumita, I. (2005). Rayleigh–Taylor instability of a particle packed viscous fluid: implications for a solidifying magma. *Geophysical Research Letters* **32**, L03309.

Moore, G., Vennemann, T. & Carmichael, I. (1998). An empirical model for the solubility of H_2O in magmas to 3 kilobars. *American Mineralogist* **83**, 36–42.

Moore, J. & Evans, B. (1967). The role of olivine in the crystallization of prehistoric Makaopuhi lava lake, Hawaii. *Contributions to Mineralogy and Petrology* **15**, 202–223.

Nagao, S. (1957). The Cretaceous formation in the East Hokkaido. *Studies of Late Mesozoic in Japan* **5**, 43–46.

Nakamura, Y. & Kushiro, I. (1970). Compositional relations of coexisting orthopyroxene, pigeonite and augite in a tholeiitic andesite from Hakone volcano. *Contributions to Mineralogy and Petrology* **26**, *265–275*.

Pecora, W. T. (1941). Structure and petrology of the Boxelder laccolith, Bearpaw Mountains, Montana. *Geological Society of America Bulletin* **52**, 817–854.

Philpotts, A. R., Carrol, M. & Hill, J. M. (1996). Crystal-mush compaction and the origin of pegmatitic segregation sheets in a thick flood-basalt flow in the Mesozoic Hartford Basin, Connecticut. *Journal of Petrology* **37**, 811–836.

Philpotts, A. R., Shi, J. & Brustman, C. (1998). Role of plagioclase crystal chains in the differentiation of partly crystallized basaltic magma. *Nature* **395**, 343–346.

Richardson, J. & Meikle, R. (1961). Sedimentation and fluidization: part III. The sedimentation of uniform fine particles and of two-component mixtures of solids. *Transactions of the Institution of Chemical Engineers* **39**, 348–356.

Richardson, J. F. & Zaki, W. N. (1954). Sedimentation and fluidization: Part I. *Transactions of the Institution of Chemical Engineers* **32**, 35–53.

Richardson, S. (1979). Chemical variation induced by flow differentiation in an extensive Karoo dolerite sheet, Southern Nambia. *Geochimica et Cosmochimica Acta* **43**, 1433–1441.

Rieke, H. H. I. & Chillingarian, G. V. (1974). Compaction of argillaceous sediments, Developments in Sedimentology 16, Elsevier, Amsterdam.

Rogan, W., Blake, S. & Smith, I. (1996). *In situ* chemical fractionation in thin basaltic lava flows: examples from the Auckland volcanic field, New Zealand, and a general physical model. *Journal of Volcanology and Geothermal Research* **74**, 89–99.

Rudman, M. (1992). Two-phase natural convection: implications for crystal settling in magma chambers. *Physics of the Earth and Planetary Interiors* **72**, 153–172.

Saffman, P. (1973). On the settling speed of free and fixed suspensions. *Studies in Applied Mathematics* **52**, 115–127.

Sasa, Y. (1957). The geology of Shikotan Islands. *Report of Geology in Hokkaido* **34**, 28.

Sasa, Y. & Hayashi, I. (1952). Oscillation mechanism in Cretaceous and Tertiary Era in the Eastern Kushiro Coal area. *Journal of Geology (Chishitu Zassi)* **58**, 292.

Schwindinger, K. R. (1999). Particle dynamics and aggregation of crytals in a magma chamber with application to Kilauea Iki olivines. *Journal of Volcanology and Geothermal Research* **88**, 209–238.

Shaw, H. R. (1965). Comments on viscosity, crystal settling, and convection in granitic magmas. *American Journal of Science* **263**, 120–152.

Shaw, H. R. (1972). Viscosities of magmatic silicate liquids: an empirical method of prediction. *American Journal of Science* **272**, 870–893.

Shaw, H. R., Wright, T. L., Peck, D. L. & Okamura, R. (1968). The viscosity of basaltic magma: an analysis of field measurements in Makaopuhi lava lake, Hawaii. *American Journal of Sciences* **266**, 225–264.

Shibata, K. (1985). The radio isotopic age in Cretaceous: about geological age determination. *Memoirs of the Geological Society of Japan* **26**, 119–133.

Simakin, A., Schmeling, H. & Trubitsyn, V. (1997). Convection in melts due to sedimentary crystal flux from above. *Physics of the Earth and Planetary Interiors* **102**, 185–200.

Simura, R. (2004). Mechanism of thermal and chemical evolution of a sheet-like magma body: constraints from the Nosappu-misaki intrusion, Northern Japan. Ph.D. thesis, University of Tokyo.

Smith, T. (1965). The differential sedimentation of particles of two different sizes. *Transactions of the Institution of Chemical Engineers* **43**, T69–T73.

Smith, T. (1966). The sedimentation of particles having a dispersion of sizes. *Transactions of the Institution of Chemical Engineers* **44**, T153–T157.

Stimson, M. & Jeffery, G. (1926). The motion of two spheres in a viscous fluid. *Proceedings of the Royal Society of Edinburgh, Section A* **111**, 110–116.

Stokes, G. (1851). On the effect of the internal friction on the motion of pendulums. *Transactions of the Cambridge Philosophical Society* **9**, 8–106.

Sugawara, T. (2000). Thermodynamic analysis of Fe and Mg partitioning between plagioclase and silicate liquid. *Contributions to Mineralogy and Petrology* **138**, 101–113.

Takahashi, S. (1978). Petrology of alkali dolerite in Nemuro Peninsula. M.Sc. thesis, Hokkaido University, Sappro, Japan.

Ueda, Y. & Aoki, K. (1968). K–Ar age in Nemuro Peninsula. *Journal of Mineralogy, Petrology and Economic Geology* **59**, 230–235.

Wacholder, E. & Sather, N. (1974). The hydrodynamic interaction of two unequal spheres moving under gravity through quiescent viscous fluid. *Journal of Fluid Mechanics* **65**, 417–437.

Wallis, G. (1969). *One-dimensional Two-phase Flow*. New York: McGraw–Hill.

Weiland, R. H., Fessas, Y. P. & Ramarao, B. V. (1984). On instabilities arising during sedimentation of two-component mixtures of solids. *Journal of Fluid Mechanics* **142**, 383–389.

Whitmore, R. L. (1955). The sedimentation of suspensions of spheres. *British Journal of Applied Physics* **6**, 239–245.

Wilshire, H. G. (1967). The Prospect alkaline diabase–picrite intrusion, New South Wales, Australia. *Journal of Petrology* **8**, 97–163.

Yagi, K. (1969). Petrology of the Alkaline Dolerite of the Nemuro Peninsula, Japan. *Geological Society of America, Memoirs* **115**, 103–147.

Yoshida, T., Yamaguchi, T. & Kawasaki, Y. (1981). Internal structure of Kutsugata lava flow Rishiri volcano (in Japanese with English abstract). *Journal of Mineralogy, Petrology and Economic Geology* **76**, 181–194.